This is to certify that the
thesis entitled

MODELING AND CONTROL OF ATOMIC FORCE MICROSCOPE FOR IMAGING USING HIGH ORDER HARMONIC MODES

presented by

Chinwe Pamela Nyenke

has been accepted towards fulfillment
of the requirements for the

Master of Science	degree in	Electrical Engineering

Major Professor's Signature

3/2/07

Date

DATE DUE	DATE DUE	DATE DUE

MODELING AND CONTROL OF ATOMIC FORCE MICROSCOPE FOR IMAGING USING HIGH ORDER HARMONIC MODES

By

Chinwe Pamela Nyenke

A THESIS

Submitted to
Michigan State University
in partial fulfillment of the requirements
for the degree of

MASTER OF SCIENCE

Department of Electrical and Computer Engineering

2007

ABSTRACT

MODELING AND CONTROL OF ATOMIC FORCE MICROSCOPE FOR IMAGING USING HIGH ORDER HARMONIC MODES

By

Chinwe Pamela Nyenke

This research assesses the imaging of specimen surface features using higher flexural modes associated with the oscillation of the atomic force microscope (AFM) cantilever. A computer simulation based on the Euler-Bernoulli Beam Equation is designed to measure variations in the oscillation amplitude due to variations in the specimen surface. The results are then compared to those of an experiment employing a real AFM and lock-in amplifier. Both simulation and experimental results demonstrate that examining higher modes yields more accurate information about a specimen surface property – particularly elasticity and topography – which is consistent with previous studies. More importantly, this research achieves improved sensitivity to surface information in lower modes when exciting the cantilever at a higher resonance frequency. The latter finding eliminates the need to extract and enhance the amplitude of higher modes, which are magnitudes smaller and consequently more difficult to measure and analyze.

ACKNOWLEDGMENTS

The author would like to thank Dr. Ning Xi in the Department of Electrical and Computer Engineering for his productive discussions and guidance in completing this project. The author also acknowledges Jiangbo Zhang for his assistance in modeling the cantilever dynamics and providing AFM image results. This research was supported by Michigan State University.

TABLE OF CONTENTS

LIST OF FIGURES vi

1. INTRODUCTION 1
1.1 BACKGROUND AND MOTIVATION 1
1.2 BRIEF OVERVIEW OF PREVIOUS WORK 2
1.3 BRIEF SUMMARY OF PROPOSED PROJECT 3
1.4 ORGANIZATION OF THE THESIS 4

2. LITERATURE REVIEW 5

3. MODELING OF AFM TAPPING MODE 8
3.1 INTRODUCTION TO TAPPING MODE 8
3.2 INFINITE DIMENSION MODEL 9
3.3 MODE VERIFICATION 14

4. COMPUTER SIMULATION STUDIES 16
4.1 SIMULATION PACKAGE 16
4.2 SIMULATION RESULTS 17
4.2.2. Response to Change in Sample Stiffness 18
4.2.2. Response to Change in Sample Topography 42
4.2.3. Multiple Changes in Sample Topography 78
4.3 DISCUSSION 88
4.3.1. Response to a Change in Sample Stiffness 88
4.3.2. Response to a Change in Sample Topography 88
4.3.3. Multiple Changes in Sample Topography 89

5. EXPERIMENT IMPLEMENTATION AND TESTING 90
5.1 DESCRIPTION OF EXPERIMENT IMPLEMENTATION 90
5.2 EXPERIMENTAL RESULTS 90
5.3 DISCUSSION 92

6. CONCLUSION AND FUTURE WORK 93
6.1 CONCLUSION 93
6.2 FUTURE WORK 93

7. APPENDIX: COMPUTER SIMULATION CODE 95

8. REFERENCES 105

LIST OF FIGURES

Figure 1. Illustration of cantilever-tip ensemble, photodetector, laser, specimen and piezotube. 1

Figure 2. AFM image of an electrode during the tapping mode. 8

Figure 3. The cantilever dimensions: A = area = WH. 9

Figure 4. Control loop model of the AFM tapping mode system in Simulink 17

Figure 5. Variations in the Young's modulus of a specimen 19

Figure 6. Point-mass model: tip displacement while scanning a sample of constant stiffness (70GPa). 22

Figure 7. Point-mass model: tip displacement while scanning a sample of varying stiffness (20-70GPa). 23

Figure 8. Point-mass model: tip displacement while scanning a sample of varying stiffness (2Pa-70GPa). 23

Figure 9. Elastic-beam model, cantilever driven at the 1st mode: tip displacement while scanning a sample of constant stiffness (70GPa). 25

Figure 10. Elastic-beam model, cantilever driven at the 1st mode: tip displacement while scanning a sample of varying stiffness (20-70GPa). 28

Figure 11. Elastic-beam model, cantilever driven at the 1st mode: tip displacement while scanning a sample of varying stiffness (2Pa-70GPa). 32

Figure 12. Elastic-beam model, cantilever driven at the 2nd mode: tip displacement while scanning a sample of constant stiffness (70GPa). 34

Figure 13. Elastic-beam model, cantilever driven at the 2nd mode: tip displacement while scanning a sample of varying stiffness (20-70GPa). 37

Figure 14. Elastic-beam model, cantilever driven at the 2nd mode: tip displacement while scanning a sample of varying stiffness (2Pa-70GPa). 40

Figure 15. Variations in sample topography. 44

Figure 16. Point-mass model: tip displacement while scanning a flat sample surface (height of -22.7nm). 49

Figure 17. Point-mass model: tip displacement while scanning a varying sample surface height (-22.7nm to -4.5nm). 50

Figure 18. Point-mass model: tip displacement while scanning a varying sample surface height (-22.7nm to -4nm). 51

Figure 19. Point-mass model: tip displacement while scanning a varying sample surface height (-22.7nm to 0nm). 52

Figure 20. Elastic-beam model driven at 1st mode: tip displacement while scanning a flat sample surface (-22.7nm) 54

Figure 21. Elastic-beam model driven at 1st mode: tip displacement while scanning a varying sample surface height (-22.7nm to -4nm). 57

Figure 22. Elastic-beam model driven at 1st mode: tip displacement while scanning a varying sample surface height (-22.7nm to -4.5nm). 60

Figure 23. Elastic-beam model driven at 1st mode: tip displacement while scanning a varying sample surface height (-22.7nm to 0nm). 63

Figure 24. Elastic-beam model driven at 2nd mode: tip displacement while scanning a flat sample surface (-22.7nm). 67

Figure 25. Elastic-beam model driven at 2nd mode: tip displacement while scanning a varying sample surface height (-22.7nm to -4.5nm). 70

Figure 26. Elastic-beam model driven at 2nd mode: tip displacement while scanning a varying sample surface height (-22.7nm to -4nm). 73

Figure 27. Elastic-beam model driven at 2nd mode: tip displacement while scanning a varying sample surface height (-22.7nm to 0nm). 76

Figure 28. Point-mass model: bulge and depression in sample surface. 80

Figure 29. Elastic-beam model driven at 1st mode: bulge and depression in sample surface and 2nd mode amplitude. 83

Figure 30. Elastic-beam model driven at 2nd mode: bulge and depression in sample surface and 1st mode amplitude. 86

Figure 31. Image results while exciting the cantilever at the 1st mode. (a) height information, (b) first mode amplitude, (c) second mode amplitude. 91

Figure 32. Image results while exciting the cantilever at the 2nd mode. (a) height information, (b) first mode amplitude, (c) second mode amplitude. 91

1. INTRODUCTION

1.1 BACKGROUND AND MOTIVATION

The atomic force microscope (AFM) is an instrument used to characterize a specimen on the scale of a few nanometers. It consists of a cantilever-tip ensemble which moves across the specimen surface while responding to attractive and repulsive forces underneath the tip (see Figure 1). As the cantilever bends in reaction to these forces, its deflection is measured by means of a laser beam reflected from the top of its free end onto a photodetector. This measured deflection is then used to adjust the height of the piezotube scanner and thus move the specimen closer to (or further from) the cantilever in order to maintain a constant desired force between the tip and surface. In some cases, piezoresistive cantilevers are used, as opposed to lasers and photodetectors; the piezoresistive element acts as a strain gage to detect the cantilever deflection.

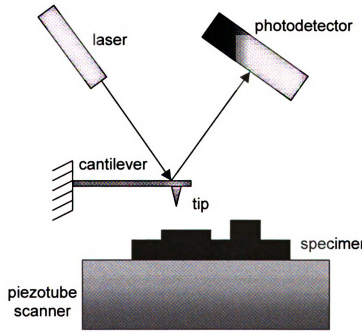

Figure 1. Illustration of cantilever-tip ensemble, photodetector, laser, specimen and piezotube.

The AFM is operated in one of three modes – contact, non-contact, and tapping – depending on the type of specimen being examined. In the contact mode, the cantilever tip is dragged across the surface such that only repulsive forces are present between the tip and specimen. The non-contact mode operation requires the cantilever to be oscillated at or near its resonance frequency while the oscillation amplitude is modified by attractive forces. (In this latter operation, a soft specimen can be scanned without dragging the tip across the surface and potentially damaging the specimen or tip.) The tapping mode combines the benefits of both contact and non-contact by allowing for high-resolution scanning and manipulation of soft specimen with minimal damage, respectively. Because of its advantages, this last operation is commonly used when investigating material properties.

The cantilever's oscillation during the tapping mode has typically been modeled as a point-mass system, which only considers the first harmonic. However, because it is actually a superposition of multiple flexural modes, researchers have questioned whether ignoring the contribution of higher harmonics results in a loss of valuable information about a specimen surface [1]-[2]. One of the current research areas in atomic force microscopy is to obtain more accurate information about the surface properties of a specimen using these higher modes, which may in turn improve imaging.

1.2 BRIEF OVERVIEW OF PREVIOUS WORK

Several studies have already demonstrated advantages to analyzing the higher harmonics, including increased image contrast and improved sensitivity to certain surface features,

such as the elastic modulus and height variation [1]-[8]. One common setback among these studies is that the amplitudes of these harmonics are magnitudes smaller than that of the first mode and, thus, require enhancement [1], [3] or implementing another method to improve measurability. Little has been done with exciting these higher modes such that the lower modes, which have larger magnitudes, can be used for analysis instead [4].

1.3 BRIEF SUMMARY OF PROPOSED PROJECT

Like previous studies, this one assesses the effect of using higher harmonics to image a specimen surface. More importantly, this study investigates the effect of exciting these higher modes such that lower ones may be used for detection of these properties as well. Any significant improvements in imaging that may be achieved when examining the higher modes can have serious implications for the analysis of DNA strands, protein peptides, polymer films, carbon nanotubes, and other structures in nanotechnology-related fields. Should the lower harmonics present comparable improvements, the finding would be vital in reducing the need to extract and enhance the small amplitudes of higher harmonics.

The objective of this project is to use a computer simulation to measure and compare the sensitivity of multiple modes to specimen surface information. An actual AFM is then employed to verify the results of the computer simulation study. The approach is to model the cantilever as an elastic beam, record changes in the oscillation amplitude using various harmonics, and assess the level of sensitivity to specimen properties via these changes.

1.4 ORGANIZATION OF THE THESIS

This paper presents a review of literature on previous research in Section 2; an explanation of the tapping mode and infinite dimensions of the cantilever motion in Section 3; a description of the AFM computer simulation, including results and discussion, in Section 4; a description of the experiment performed with an actual AFM, including results and discussion, in Section 5; a conclusion of the project and ideas for future work in Section 6; an appendix of simulation code and further results in Section 7; and a list of references used for this research in Section 8.

2. LITERATURE REVIEW

There has been speculation that modeling the cantilever as a point mass, or a system with only one vibration mode, potentially limits the accuracy of information obtained about a given specimen surface. Thus, researchers are beginning to consider the higher harmonics that contribute to the cantilever motion during the tapping mode. By understanding that this motion is a 'superposition of several eigenmode vibrations' [1]-[2], such properties as surface stiffness and topography may be detected more accurately. Recent work by several researchers demonstrates that analyzing the higher modes of the cantilever motion may improve sensitivity to certain specimen properties that might otherwise go unnoticed when analyzing the first mode alone.

Hillenbrand, M. Stark, R. W. Stark, and Heckl have all investigated the use of higher modes to increase image contrast. Hillenbrand and M. Stark collaborated to evaluate the detection of tip-specimen interaction variations on an etched silicon wafer. Their results demonstrated that higher harmonics, particularly the 13th, are more sensitive to deviations in the time and strength of tip-specimen interaction and, thus, to deviations on the wafer surface [5]. A few years later, R. W. Stark refined the findings of this previous study by determining that variations in specimen topography and elasticity are accurately detected by the 8th and 13th mode, respectively [6]. One minor shortcoming in both references is that the experimental data is mainly qualitative; visual comparisons of distinctions in image results are used to assess the sensitivity of each harmonic to specimen properties. R. W. Stark attributes the lack of quantitative data in his work to the low bandwidth of the lock-in amplifier equipment which limited the ability to

measure the small amplitudes of the higher harmonics. Nevertheless, both references show increased image contrast when looking beyond the first vibration mode.

Higher harmonics have yielded improvements in areas beyond image contrast as demonstrated in studies by Sahin, Rodriguez, and Garcia. Sahin reveals that hard and soft samples can be investigated more accurately with the 24th and 8th harmonic, respectively [1]. Unlike R.W. Stark, he obtains more quantitative results and examines the detection of elasticity (rather than the detection of *variations* in elasticity) for a given specimen. However, in order to accomplish this task, Sahin implements a method of using specially-designed cantilevers to enhance the small amplitude signals of higher modes. Meanwhile, Rodriguez and Garcia show that the second harmonic can detect very small force variations such that they are then able to sense changes in the atom and molecule composition of the specimen [7]. This work seems inconsistent with that of R.W. Stark, Hillenbrand, and Sahin, who all suggest that modes below the 8th omit valuable information about material properties. However, Rodriguez and Garcia present thorough quantitative data demonstrating that the second mode is sufficient, at least in detecting the atom and molecule composition by determining the Hamaker constant. Additionally, the two researchers avoid implementing a method to measure higher mode amplitudes since they only examine the first two harmonics.

The general results of the literature demonstrate advantages in exploiting the higher modes but also reveal a challenge in measuring the small amplitudes (or high frequency) of these modes. For this reason, this research involves the investigation of using lower

modes to detect specimen properties when exciting the cantilever at a higher resonance frequency. It is believed that these lower modes, which have larger amplitudes, can then be used for analysis. The advantages of examining higher modes are also investigated further in this research. Similar to Rodriguez and Garcia, few harmonics are used and shown to be sufficient. Unlike previous works, this project provides more experimental results.

3. MODELING OF AFM TAPPING MODE

3.1 INTRODUCTION TO TAPPING MODE

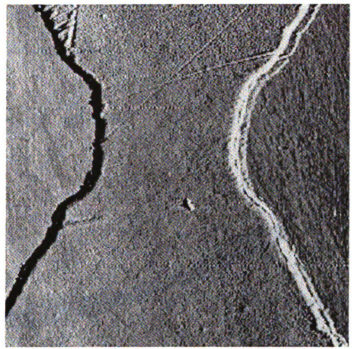

Figure 2. AFM image of an electrode during the tapping mode.

During the tapping mode, the cantilever is oscillated at or close to its fundamental resonance frequency, causing the tip to touch the specimen surface intermittently. The oscillation amplitude is used as feedback and compared to a desired constant amplitude set by the operator. Any error between the actual and desired amplitudes results in an adjustment of the piezotube scanner height and thus an adjustment in the tip-specimen separation. The error may be induced by a bulge or depression in the specimen surface which causes the oscillation amplitude of the cantilever to change in size. Figure 2 shows a tapping mode image obtained while scanning an electrode in this project.

During the tapping mode, the tip-specimen interaction force enters two attractive and repulsive regimes. In the attractive regime, the tip is far enough from the specimen surface that van der Waals' forces dominate while, in the repulsive regime, the tip is close enough to the surface such that Pauli and ionic repulsive forces dominate. On the nanometer scale, a small layer of condensed water vapor is present on the specimen surface and allows for capillary forces to also exist.

3.2 INFINITE DIMENSION MODEL

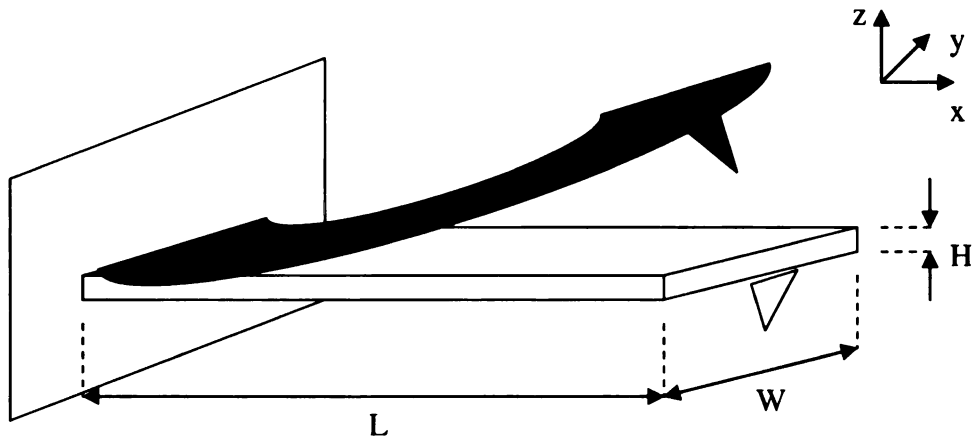

Figure 3. The cantilever dimensions: A = area = WH.

The cantilever was modeled as a long, slender linearly elastic beam with a uniform cross-section and small deformations (see Figure 3). Because of these and other modeling assumptions, the Euler-Bernoulli Beam Equation was appropriately applied to calculate the deflection w of the cantilever. The equation which describes the deflection is

$$\frac{\partial^2}{\partial x^2}\left[EI\frac{\partial^2 w(x,t)}{\partial x^2}\right] = p, \tag{1}$$

where E is the Young's modulus of the cantilever, I is the area moment of inertia, and p is the end load. Assuming that E and I are constant along the length of the cantilever, the above equation simplifies to

$$EI\frac{\partial^4 w(x,t)}{\partial x^4} = p \tag{2}$$

Since the end load p (e.g., tip-specimen interaction force) causes the cantilever to vibrate, it can be expressed using the Newton-Euler equation

$$p = -\rho A\frac{\partial^2 w(x,t)}{\partial x^2}, \tag{3}$$

where the area A and linear mass density ρ, are assumed to be constant along the length of the cantilever. Combining Equations (2) and (3) produces the following

$$EI\frac{\partial^4 w(x,t)}{\partial x^4} + \rho A\frac{\partial^2 w(x,t)}{\partial x^2} = 0 \tag{4}$$

The initial conditions for the cantilever are

$$w(x,t) = 0\,|_{t=0}, \quad \frac{\partial w(x,t)}{\partial x}\,|_{t=0} = 0 \tag{5}$$

Additionally, the fixed end of the cantilever must have zero deflection and velocity at all times. The free end should not have a bending moment or shearing force. Thus, the boundary conditions are

$$w(x,t)\,|_{x=0} = 0, \quad \frac{\partial w(x,t)}{\partial x}\,|_{x=0} = 0, \tag{6a}$$

$$EI\frac{\partial^2 w(x,t)}{\partial x^2}\,|_{x=L} = 0, \quad EI\frac{\partial^3 w(x,t)}{\partial x^3}\,|_{x=L} = 0 \tag{6b}$$

To solve Equation (4), the separation of variables method is used. We first guess that *w(x,t)* can be separated into two independent variables as follows

$$w(x,t) = \phi(x)q(t), \tag{7}$$

where one depends on space and the other on time. Plugging this solution into Equation (4) yields

$$EI\frac{\partial^4(\phi(x)q(t))}{\partial x^4} + \rho A\frac{\partial^2(\phi(x)q(t))}{\partial x^2} = 0, \tag{8}$$

Consequently, the general solution for $\phi(x)$ is (6):

$$\phi(x) = A\sin(kx) + B\cos(kx) + C\sinh(kx) + D\cosh(kx), \tag{9}$$

where $k = \sqrt[4]{\rho A/(EI)\omega^2}$. While using the boundary conditions to find the coefficients A, B, C, and D, the following frequency equation is obtained

$$\cos(kL)\cosh(kL) = -1, \tag{10}$$

There are an infinite number of k values that satisfy Equation (10) such that

$$\omega_i = k_i^2\sqrt{\frac{EI}{\rho A}}, \quad i = 1,2,3,\ldots,\infty, \tag{11}$$

where ω_i is the eigenfrequency of the ith mode. For each value k_i, there exists a ϕ_i, and thus a characteristic vibration w_i

$$w_i(x,t) = \phi_i(x)q_i(t), \tag{12}$$

The general solution to Equation (4) is a sum of the infinite number of characteristic vibrations

$$w_i(x,t) = \sum_{i=1}^{\infty} \phi_i(x)q_i(t), \tag{13}$$

Thus, by Euler-Bernoulli Beam Equation it is shown that the cantilever vibrates at infinite resonant frequencies simultaneously, rather than at a single frequency. During the tapping mode, the forces (driving and tip-specimen interaction) that act on the cantilever tip require a modification of Equation (4) to

$$EI\frac{\partial^4 w(x,t)}{\partial x^4} + \rho A\frac{\partial^2 w(x,t)}{\partial x^2} = F_{driving}\cos\omega t + F(t)_{tip-specimen}, \tag{14}$$

The tip-specimen forces are primarily attractive and repulsive, as described in Section 3.1. When the tip-specimen instantaneous separation d is larger than the intermolecular distance a_0, attractive forces are present and modeled as

$$F(0,d)_{ts} = -\frac{HR}{6(d^2)}, \tag{15}$$

where H is the Hamaker constant and R is the radius of the tip. When d is smaller than a_0, or when the tip is relatively close to the specimen surface, the attractive forces are now modeled as

$$F(0,d)_{ts} = -\frac{HR}{6(a_0{}^2)} \tag{16}$$

using the Derjaguin-Müller-Toporov (DMT) model [9]. In this region, repulsive forces are also present and represented with the following equation

$$F(0,d)_{ts} = -\frac{HR}{6({a_0}^2)} + \frac{4}{3}E\sqrt{R}(a_0 - d)^{3/2} \tag{17}$$

using DMT. The repulsive forces become dominant when d is smaller than a_0.

The solution to Equation (14) is still a superposition of infinite vibrations but the forces are now factors of $q(t)$. The cantilever dimensions in this experiment are: H = 4um, W = 35um, L = 120 um, and E = 130GPa. The tip radius R is 20nm and its height is negligible.

3.3 MODE VERIFICATION

An accurate measurement of the cantilever's fundamental resonance frequency is necessary for correct determination of the specimen properties during the tapping mode operation. The manufacturer typically attaches a nominal fundamental frequency f_1 to each AFM cantilever which may be a few percentages off the actual value. As a result, f_1 must be calibrated.

For this project, the Nanoscope III Tuning Software was used to calibrate f_1 (50kHz) for the cantilever in the AFM experiment. The cantilever was driven at a range of frequencies close to f_1 and the frequency response was recorded with the software. The frequency that yielded a response with the largest amplitude was then assumed to be the actual fundamental resonance frequency. For this project, that value was 51.6kHz. The same procedure was applied to the nominal second resonance frequency, which was 210kHz; the actual value was approximately 208.8kHz.

4. COMPUTER SIMULATION STUDIES

4.1 SIMULATION PACKAGE

A simulation package (Veeco Company) of the atomic force microscope during the tapping mode was used. The simulation code, which originally modeled the cantilever motion as a point-mass, was modified to account for infinite flexural modes. Tests were performed in Simulink, a platform developed by Mathworks for the simulation of dynamic systems. All tests were run on a personal computer.

Figure 4 shows a diagram of the AFM control-loop model that was run in Simulink; the cantilever block contains the software that calculates the multiple modes based on the Infinite Dimension Model in Section 3.2. (See Appendix for code.) The setpoint amplitude is a constant amplitude set by the user during a closed loop simulation of the tapping mode. The error signal between this setpoint amplitude and the actual oscillation amplitude of the cantilever is amplified by a gain and ultimately used to adjust the height of the holder position. The results in this project were obtained while running open-loop simulations of the tapping mode; the actual cantilever oscillation amplitude was monitored while the holder position remained unadjusted.

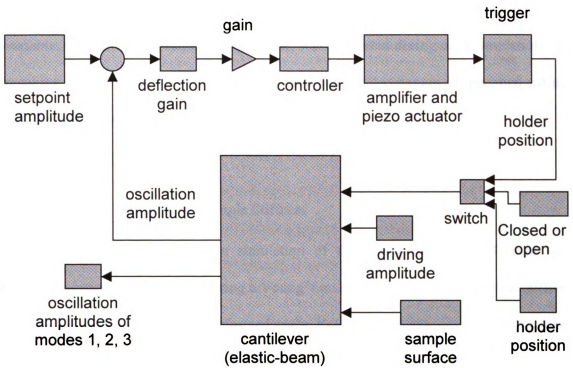

Figure 4. Control loop model of the AFM tapping mode system in Simulink

4.2 SIMULATION RESULTS

Results were obtained and compared for a point-mass and elastic-beam simulation of the cantilever motion. For the point-mass model, the simulated cantilever was driven at the first resonance frequency and only the first harmonic was analyzed. During the elastic-beam simulation, the first three harmonics were analyzed while the cantilever was first driven at the first resonance frequency and then at the second resonance frequency. Thus, three total simulations were actually performed: point-mass, elastic-beam while excited at the first resonance frequency, and elastic-beam while excited at the second resonance frequency. The accuracy of the point-mass and two elastic-beam models was investigated by running three simulation scenarios: 1) a variation in sample stiffness, 2) a

variation in sample topography, and 3) multiple variations in sample topography. One variable, the cantilever oscillation amplitude, was measured during each simulation. The resulting measurements were used to evaluate sensitivity to changes in specimen stiffness and topography as well as determine imaging accuracy.

4.2.2. Response to Change in Sample Stiffness

A 2-millisecond single-line scan simulation of the cantilever was performed on a computer-generated specimen having a Young's modulus of 70GPa, or constant stiffness. The same simulation was then performed as the Young's modulus was adjusted to 20GPa after 0.8 milliseconds of scanning and reset to 70GPa after 1.2 milliseconds to replicate a momentary change in sample stiffness. The same procedure was lastly performed for an adjustment to 2Pa to replicate a more significant change in sample stiffness. Figure 5 illustrates these changes in Young's modulus. In all cases, the fixed end of the cantilever (holder position) was set to 0nm while the specimen was simulated as flat surface with a constant height of -4nm, or 4nm below the holder position.

Figure 5. Variations in the Young's modulus of a specimen

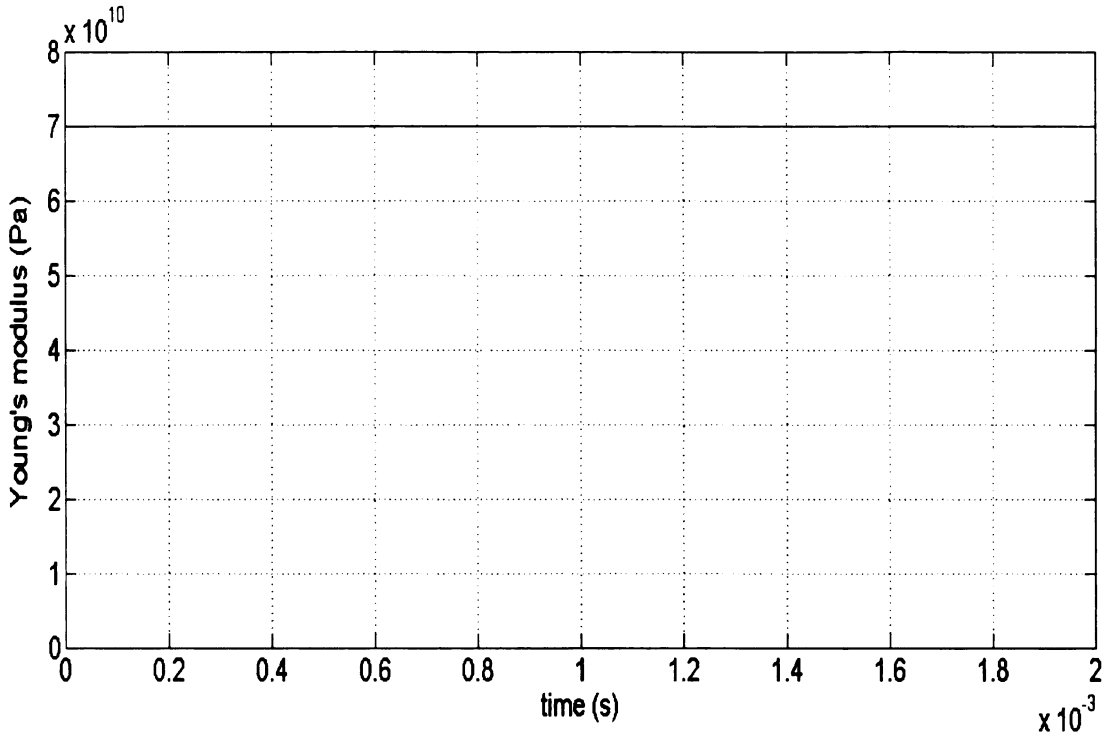
x 10^10
8
7
6
5
4
3
2
1
0
Young's modulus (Pa)
0
0.2
0.4
0.6
0.8
1
1.2
1.4
1.6
1.8
2
time (s)
x 10^-3

(a)

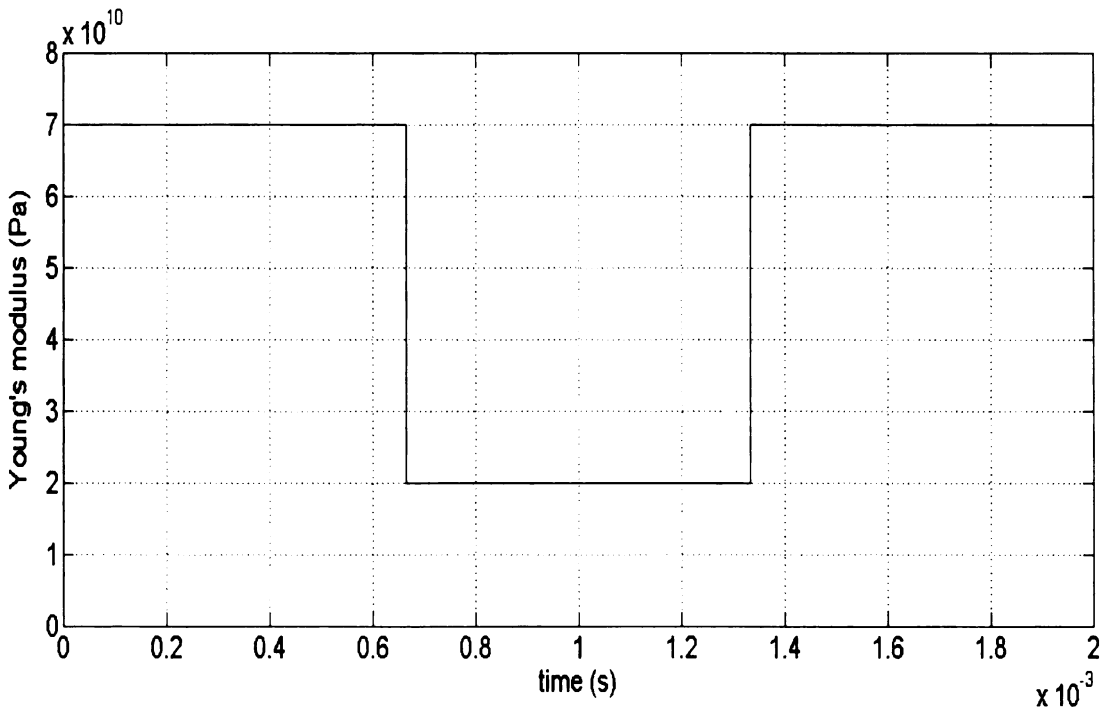
x 10^10
8
7
6
5
4
3
2
1
0
Young's modulus (Pa)
0
0.2
0.4
0.6
0.8
1
1.2
1.4
1.6
1.8
2
time (s)
x 10^-3

(b)

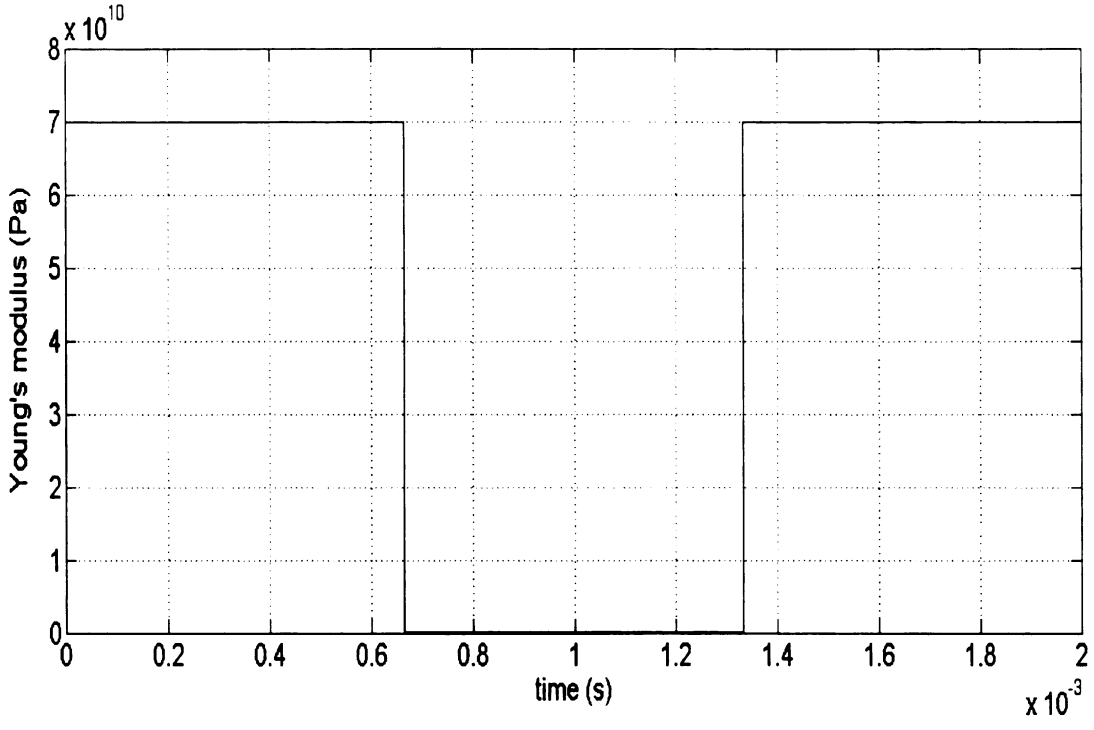

(c)

Figure 5 continued.

During the point-mass simulation, the sinusoidal driving force amplitude was set to 95nm which yielded a maximum oscillation amplitude of 8nm such that the cantilever would barely tap the flat specimen surface. This was done so that the height of the specimen would not interfere with the results of this simulation. The results of the point-mass simulation in Figure 6 demonstrate that there is no change in the oscillation amplitude as the Young's modulus remains constant, which is expected. In Figures 7 and 8, the cantilever's oscillation amplitude again remains unchanged while the stiffness decreases in the center of the specimen. Thus, the variations in sample stiffness were not detected using the first mode alone.

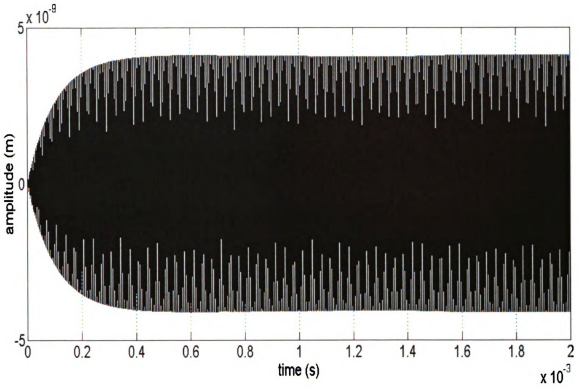

Figure 6. Point-mass model: tip displacement while scanning a sample of constant stiffness (70GPa).

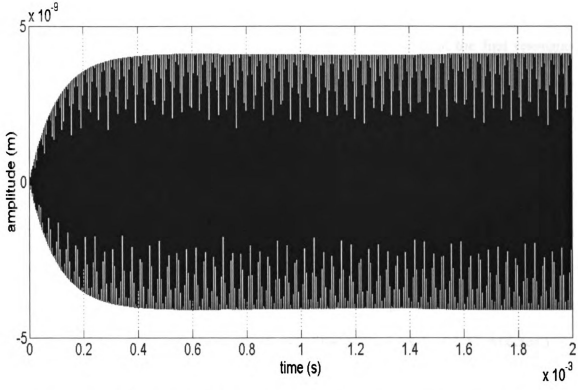

Figure 7. Point-mass model: tip displacement while scanning a sample of varying stiffness (20-70GPa).

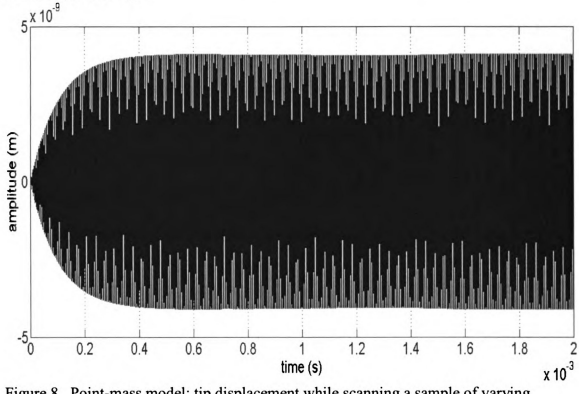

Figure 8. Point-mass model: tip displacement while scanning a sample of varying stiffness (2Pa-70GPa).

In order to evaluate the elastic-beam model, the first three flexural modes were extracted. The tip response was first recorded while driving the cantilever at the first resonance frequency for each of the three Young's modulus values. The driving force amplitude remained set at 95nm. The results in Figure 9 show that the amplitudes of each of the modes remain steady as the stiffness of the specimen remains constant, which is expected. In Figures 10 and 11, while the stiffness decreases in the center of the specimen, the mode amplitudes again remain unchanged. Despite the fact that three modes are now analyzed instead of one, the variations in surface stiffness continue to go undetected. (Note how in Figures 9-11, the first mode amplitudes for each of the three Young's modulus values are identical to those of the point-mass model, as expected.)

Figure 9. Elastic-beam model, cantilever driven at the 1st mode: tip displacement while scanning a sample of constant stiffness (70GPa).

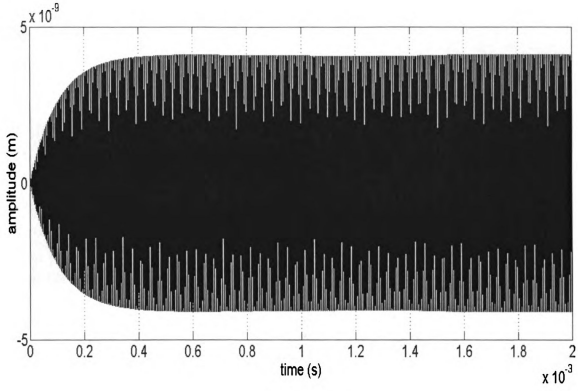

(a) first mode

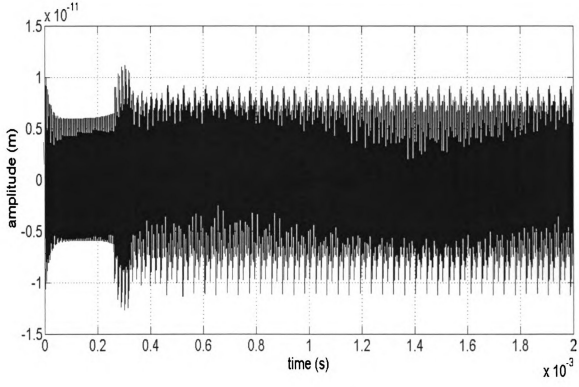

(b) second mode

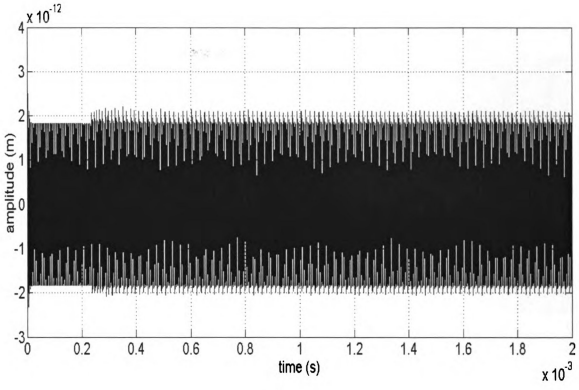

(c) third mode

Figure 9 continued.

Figure 10. Elastic-beam model, cantilever driven at the 1st mode: tip displacement while scanning a sample of varying stiffness (20-70GPa).

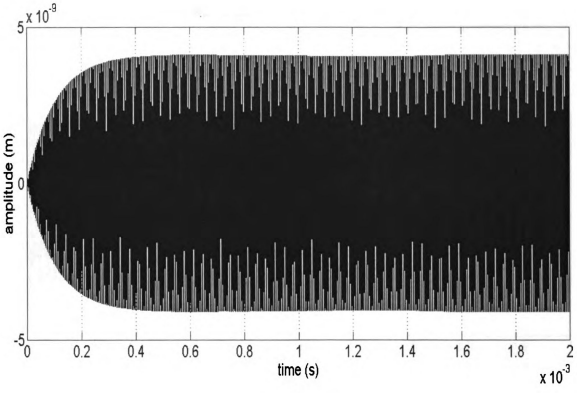

(a) first mode

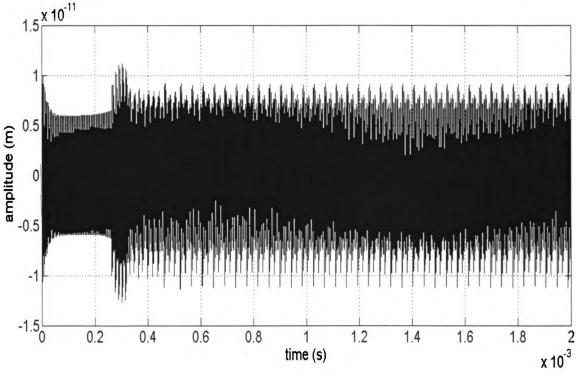

(b) second mode

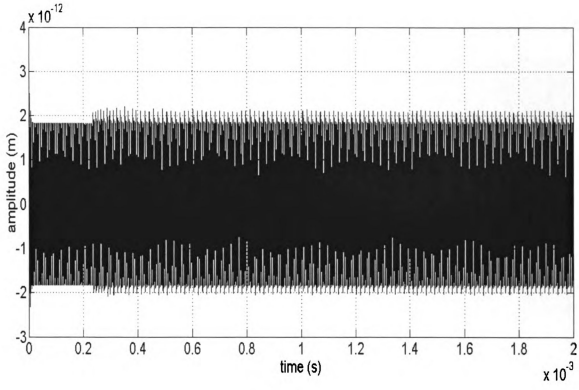

(c) third mode

Figure 10 continued.

Figure 11. Elastic-beam model, cantilever driven at the 1st mode: tip displacement while scanning a sample of varying stiffness (2Pa-70GPa).

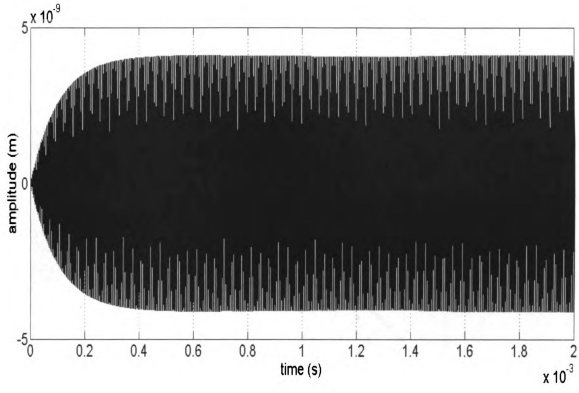

(a) first mode

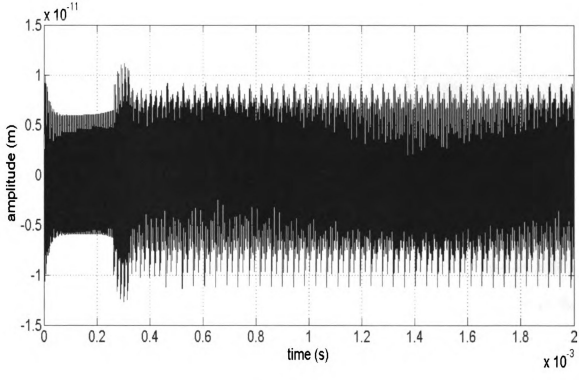

(b) second mode

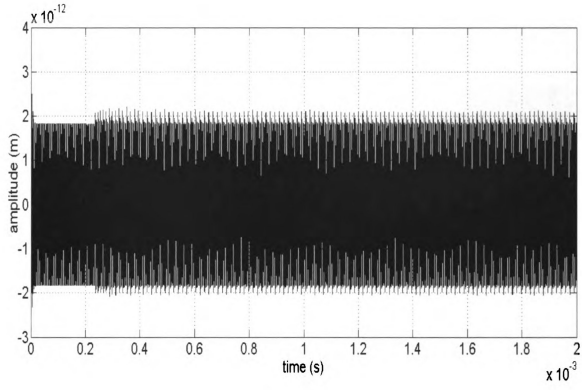

(c) third mode

Figure 11 continued.

In the second simulation for evaluating the elastic-beam model, the cantilever was driven at the second resonance frequency for each of the three Young's modulus values. The driving force amplitude was increased to 660nm to achieve the same oscillation amplitude of 8nm for the driven mode as in the previous simulations. While the Young's modulus remains a constant 70GPa during scanning, all three mode amplitudes in Figure 12 remain steady. However, when the specimen stiffness decreases momentarily to 20GPa, there is a visible change in the first mode amplitude (see Figure 13). When the Young's modulus decreases to 2 Pa, this amplitude change becomes more significant and a slight amplitude variation begins to appear in third mode (see Figure 14).

Figure 12. Elastic-beam model, cantilever driven at the 2nd mode: tip displacement while scanning a sample of constant stiffness (70GPa).

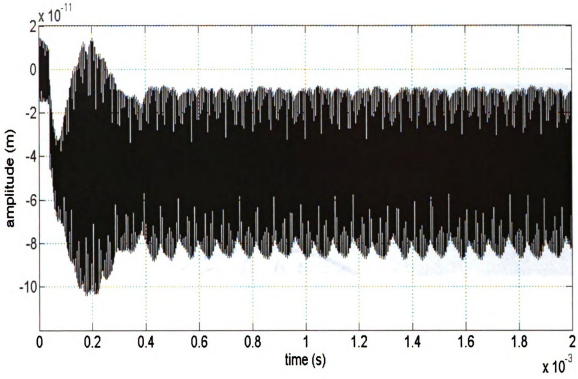

(a) first mode

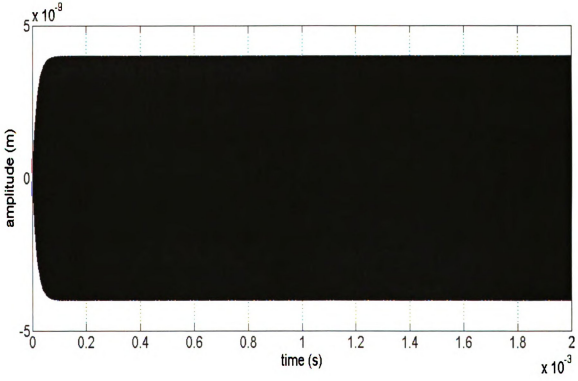

(b) second mode

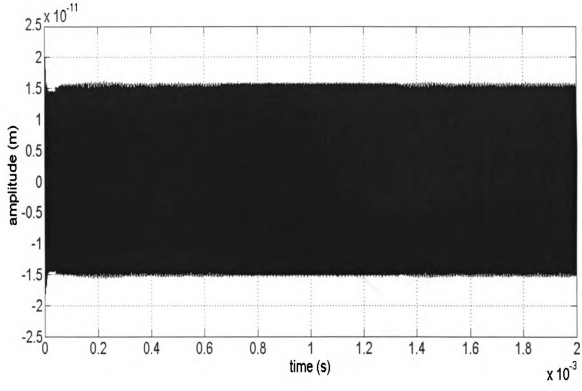

(c) third mode

Figure 12 continued.

Figure 13. Elastic-beam model, cantilever driven at the 2nd mode: tip displacement while scanning a sample of varying stiffness (20-70GPa).

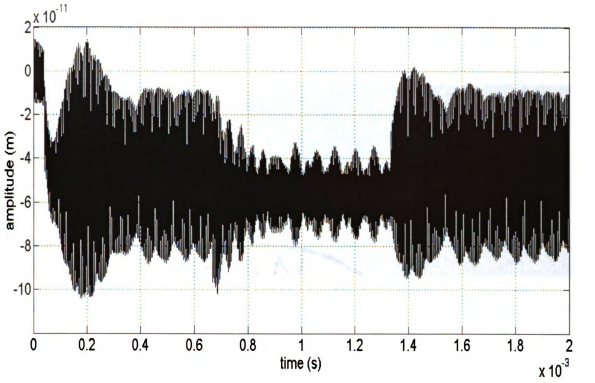

(a) first mode

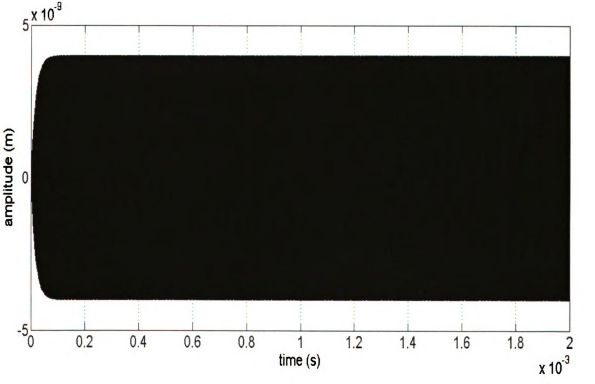

(b) second mode

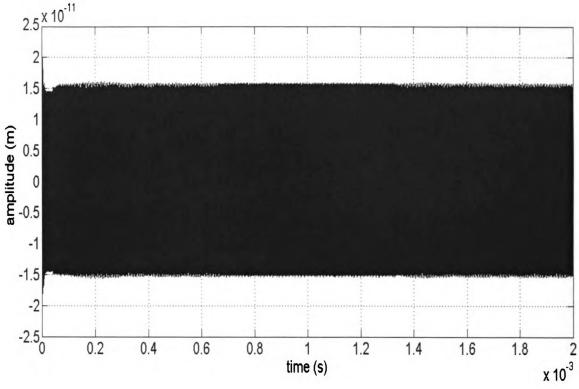

(c) third mode

Figure 13 continued.

Figure 14. Elastic-beam model, cantilever driven at the 2nd mode: tip displacement while scanning a sample of varying stiffness (2Pa-70GPa).

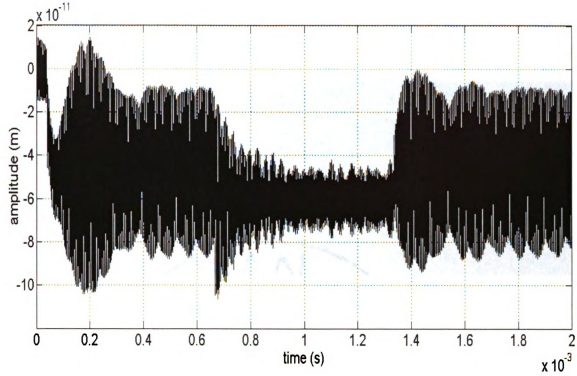

(a) first mode

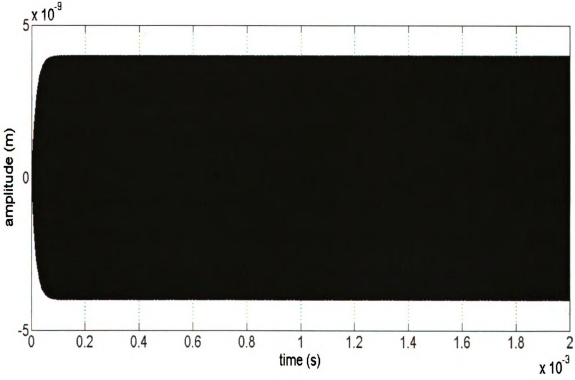

(b) second mode

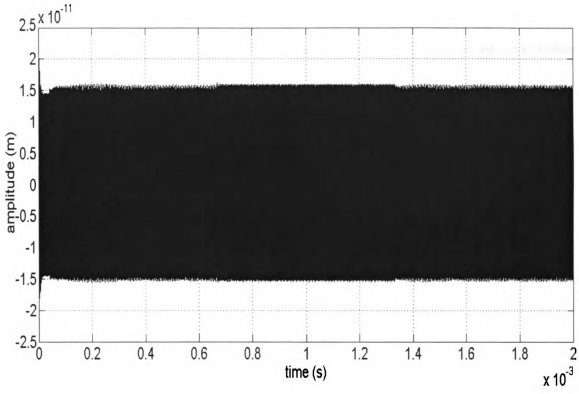

(c) third mode

Figure 14 continued.

4.2.2. Response to Change in Sample Topography

For this scenario, a 2-millisecond single-line scan simulation was performed on a computer-generated flat specimen surface with a constant height of -22.7nm (i.e., 22.7nm below the holder position). The height was chosen to give the cantilever ample room to move and reach its maximum oscillation amplitude of 8nm. A simulation was then performed on a specimen surface that was adjusted to -4.5nm after 0.7 milliseconds of scanning and reset to -22.7nm after 1.4 milliseconds to replicate a momentary change in specimen height. The procedure was repeated for surface height adjustments to -4nm and

0nm. Figure 15 illustrates these four computer-generated specimen surfaces. All simulations were run using a sample of constant stiffness (70GPa) and a cantilever holder fixed at 0nm.

Figure 15. Variations in sample topography.

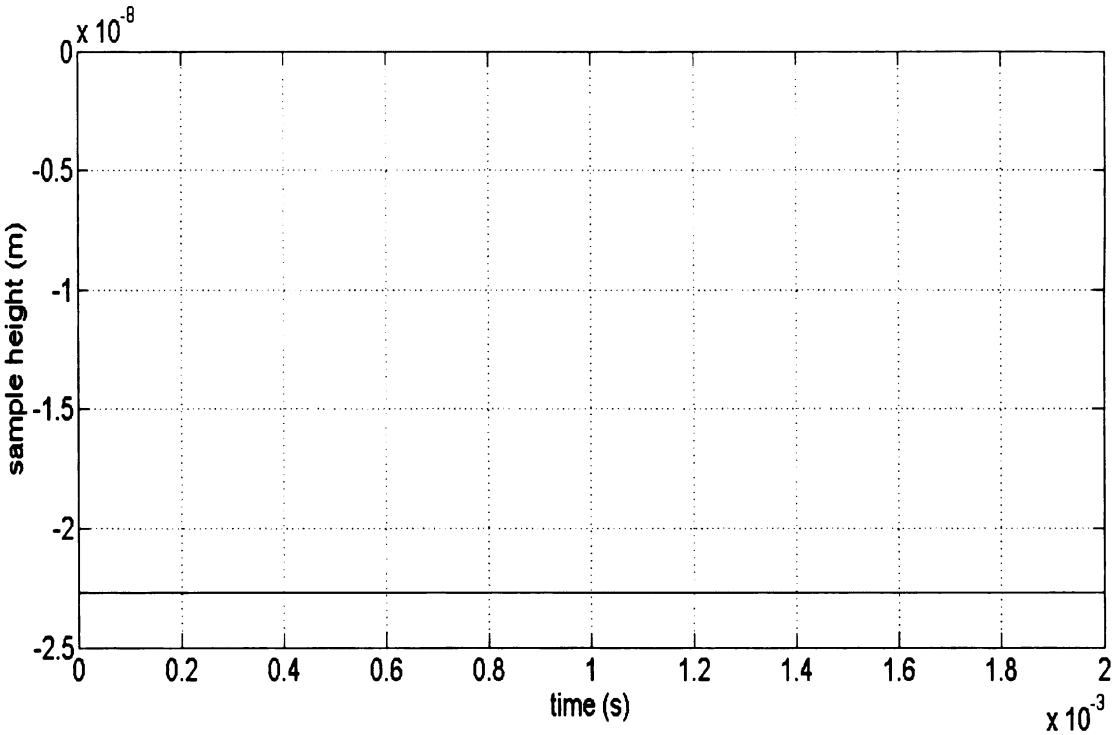
x 10^-8
0
-0.5
-1
-1.5
-2
-2.5
sample height (m)
0
0.2
0.4
0.6
0.8
1
1.2
1.4
1.6
1.8
2
time (s)
x 10^-3

(a)

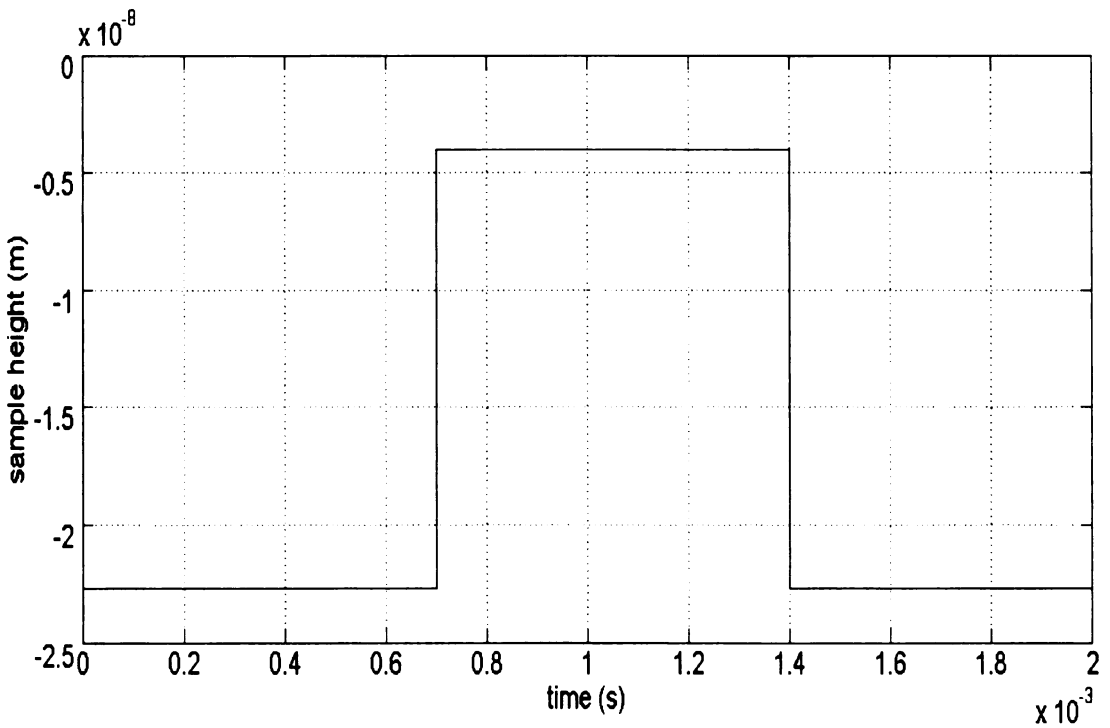
x 10^-8
0
-0.5
-1
-1.5
-2
-2.5
sample height (m)
0
0.2
0.4
0.6
0.8
1
1.2
1.4
1.6
1.8
2
time (s)
x 10^-3

(b)

Figure 15 continued.

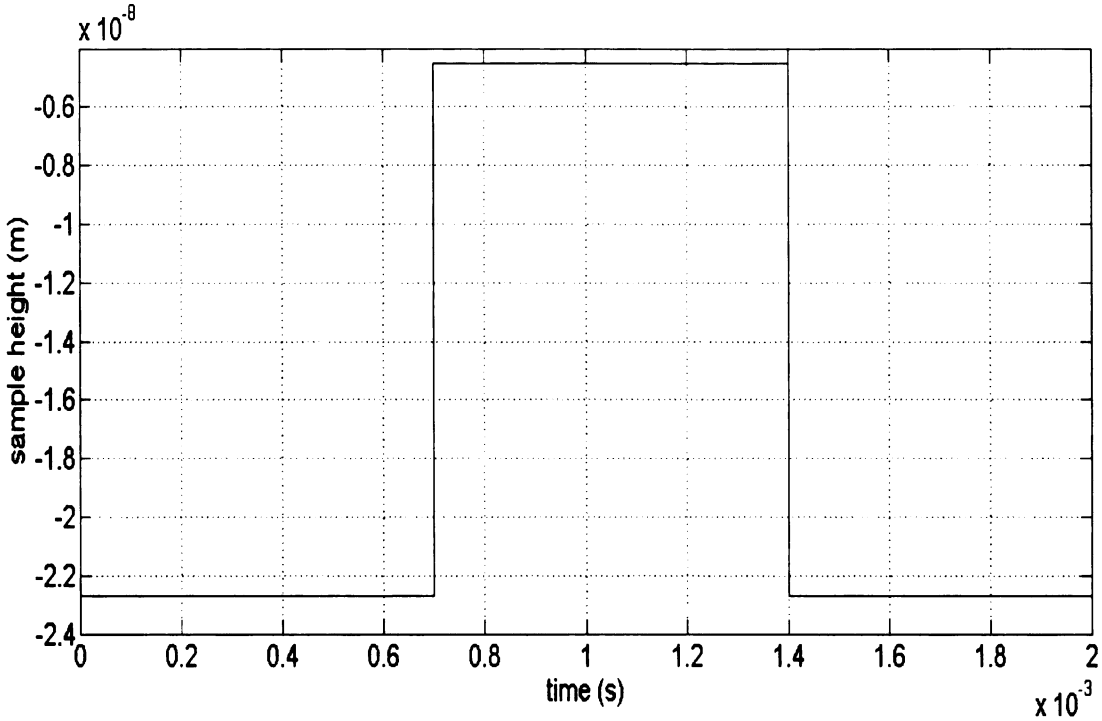
x 10^-8
-0.6
-0.8
-1
-1.2
-1.4
-1.6
-1.8
-2
-2.2
-2.4
sample height (m)
0
0.2
0.4
0.6
0.8
1
1.2
1.4
1.6
1.8
2
time (s)
x 10^-3

(c)

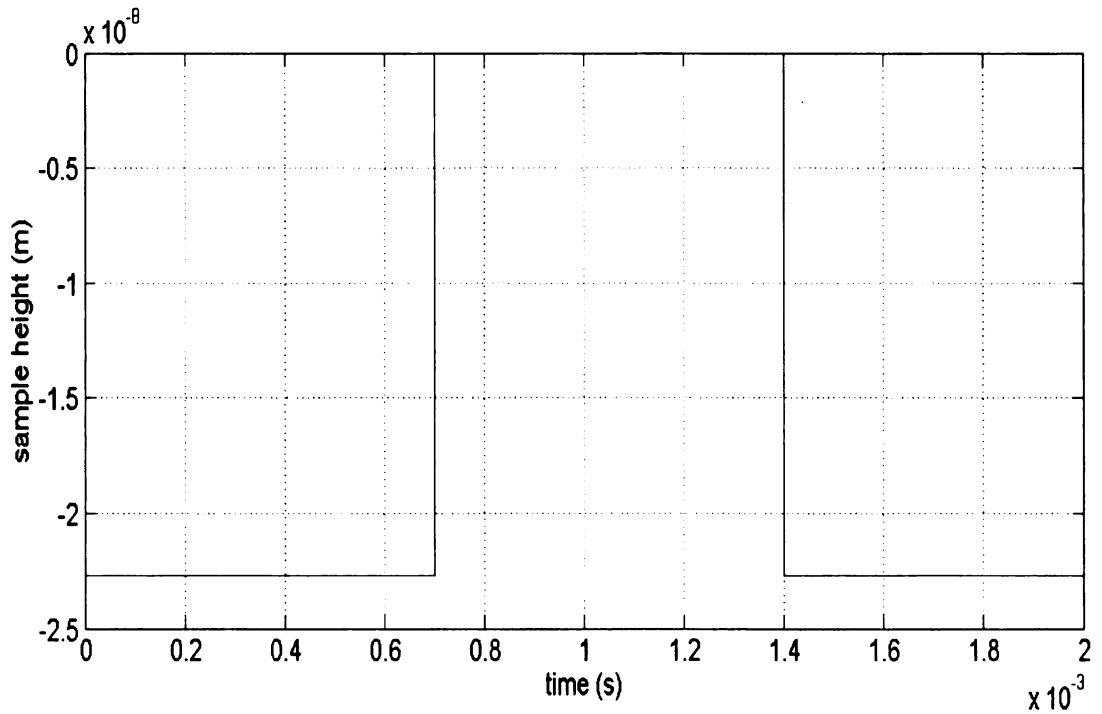
x 10^-8
0
-0.5
-1
-1.5
-2
-2.5
sample height (m)
0
0.2
0.4
0.6
0.8
1
1.2
1.4
1.6
1.8
2
time (s)
x 10^-3

(d)

In order to evaluate the point-mass model, a simulation was performed on the four samples shown in Figure 15 while extracting only the first mode of vibration. The results in Figure 16 show a steady oscillation amplitude as the specimen surface remains flat, which is expected. In Figure 17, the amplitude remains fairly constant despite the presence of a slight bulge on the specimen surface. It is only when the bulge is large enough to restrict the tip displacement that the oscillation amplitude decreases (see Figure 18); this occurs when the separation between the bulge and the cantilever's rest position is 4nm. As the bulge on the specimen surface increases in height, the first mode oscillation amplitude changes more significantly. When the bulge height is 0nm, or at the same height as the cantilever's rest position, the amplitude is approximately zero because the cantilever is entirely obstructed and unable to vibrate (see Figure 18).

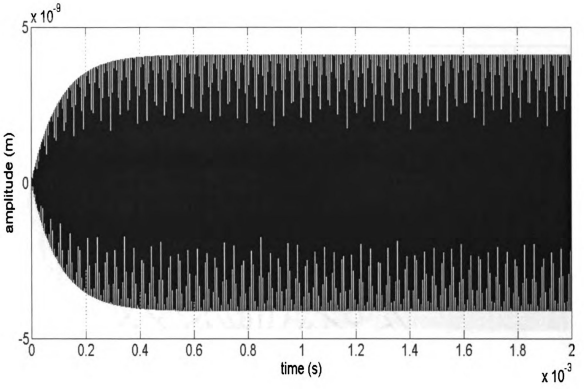

Figure 16. Point-mass model: tip displacement while scanning a flat sample surface (height of -22.7nm).

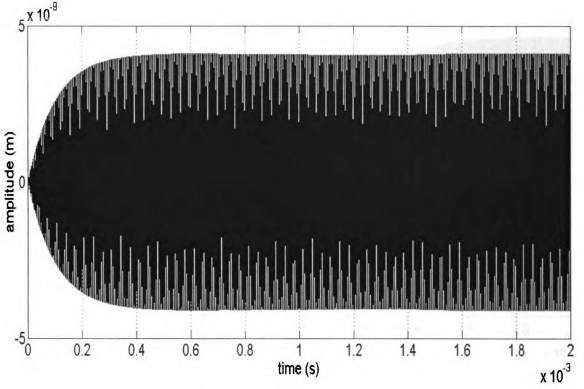

Figure 17. Point-mass model: tip displacement while scanning a varying sample surface height (-22.7nm to -4.5nm).

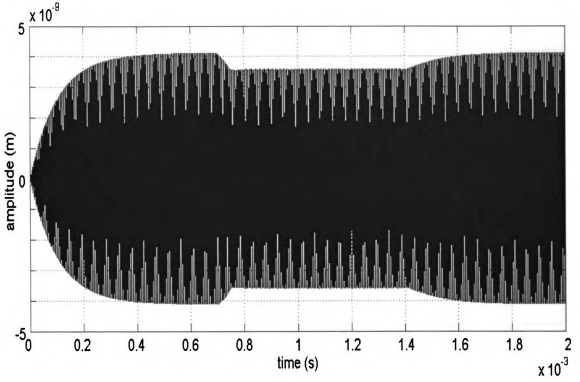

Figure 18. Point-mass model: tip displacement while scanning a varying sample surface height (-22.7nm to -4nm).

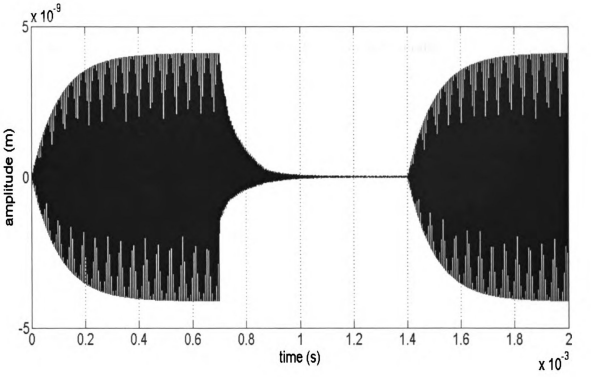

Figure 19. Point-mass model: tip displacement while scanning a varying sample surface height (-22.7nm to 0nm).

In order to evaluate the elastic-beam model, the first three flexural modes were extracted. In the first simulation, the cantilever was driven at the first resonance frequency and the oscillation amplitude was recorded for each mode during each variation in surface height. In Figure 20, the results show steady mode amplitudes when scanning a flat sample surface as expected. However, the second and third mode amplitudes become increasingly sensitive to changes in surface height starting at -4.5nm (see Figures 20-23). The first mode amplitude is only affected when the tip starts to impede the surface at 4nm below the holder position, as in the case of the point-mass simulation. Amplitude changes in all three modes are most significant when the surface is at the same height as

the cantilever holder. (Note that the amplitudes of the undriven modes – second and third – are magnitudes smaller than that of the driven, or first, mode).

Figure 20. Elastic-beam model driven at 1st mode: tip displacement while scanning a flat sample surface (-22.7nm).

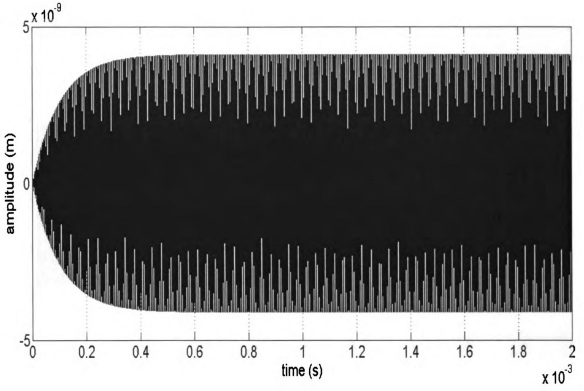

(a) first mode

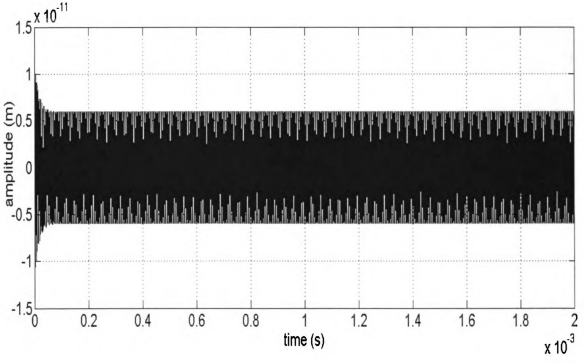

(b) second mode

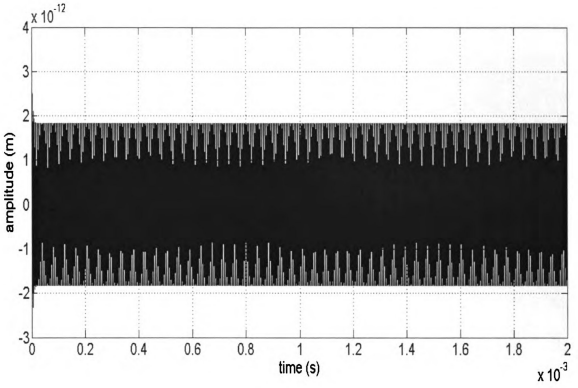

(c) third mode

Figure 20 continued.

Figure 21. Elastic-beam model driven at 1st mode: tip displacement while scanning a varying sample surface height (-22.7nm to -4nm).

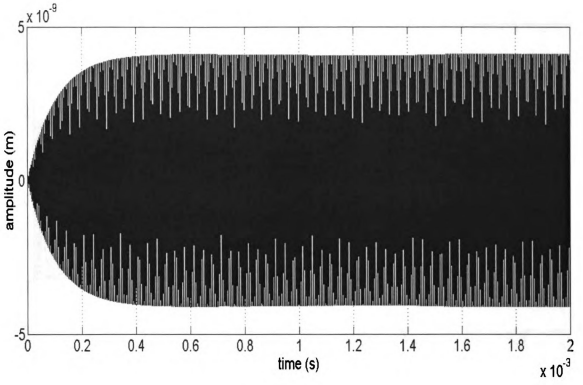

(a) first mode

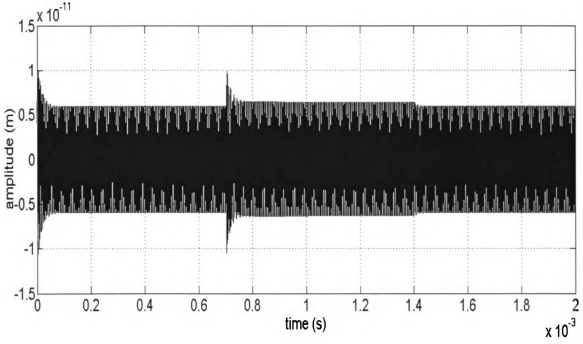

(b) second mode

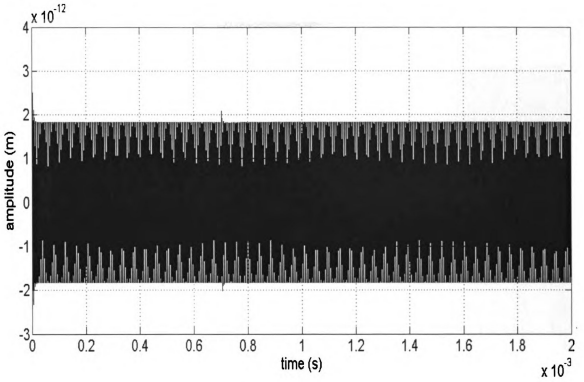

(c) third mode

Figure 21 continued.

Figure 22. Elastic-beam model driven at 1st mode: tip displacement while scanning a varying sample surface height (-22.7nm to -4.5nm).

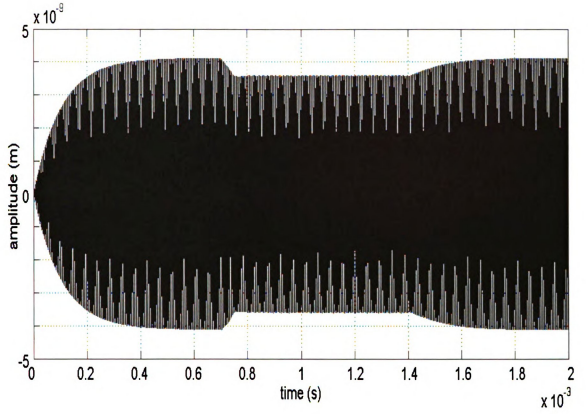

(a) first mode

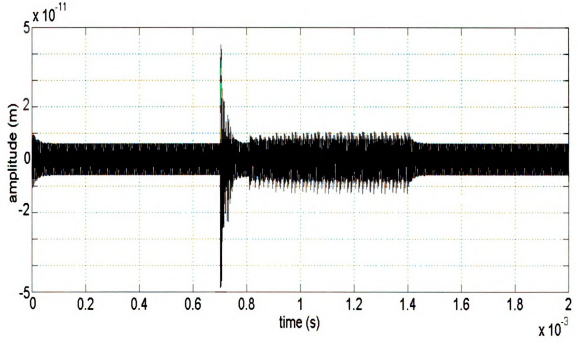

(b) second mode

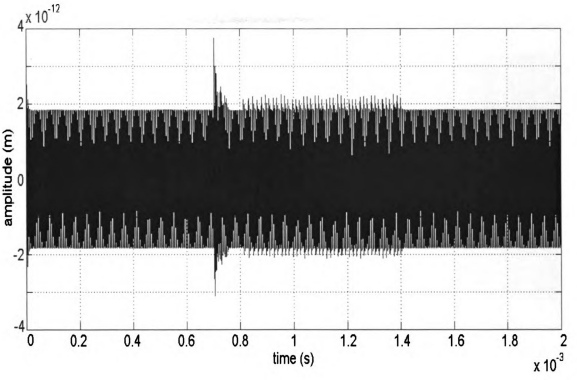

(c) third mode

Figure 22 continued.

Figure 23. Elastic-beam model driven at 1st mode: tip displacement while scanning a varying sample surface height (-22.7nm to 0nm).

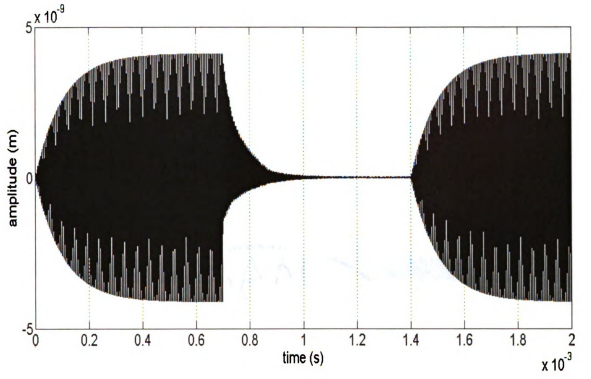

(a) first mode

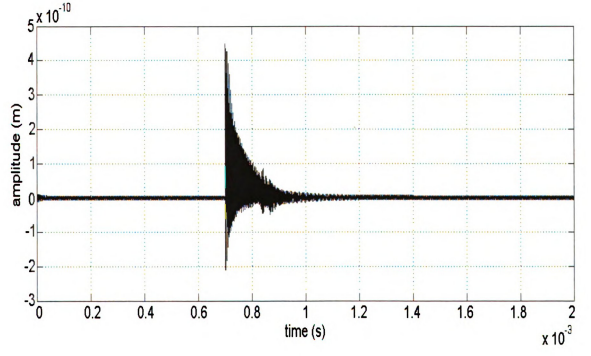

(b) second mode

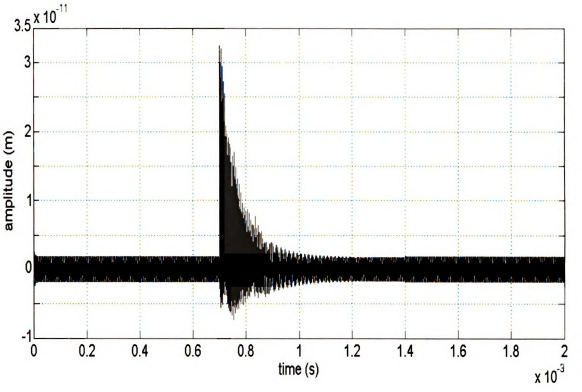

(c) third mode

Figure 23 continued.

In a second simulation for evaluating the elastic-beam model, the cantilever was driven at the second resonance frequency during each of the four sample height variations. When the sample surface is flat, the amplitude of each the three modes remains steady as expected (see Figure 24). However, the first and third mode amplitudes show an increasing sensitivity to changes in surface height (see Figures 24-27). In Figure 25, the first mode is able to detect the surface height adjustment of 4.5nm below the holder position. Amplitude changes are significant in both the first and third modes and barely visible in the second mode when the surface height is adjusted closer to the cantilever at 4 nm below the holder position (see Figure 26). In Figure 27, amplitude changes in all

three modes are most significant when the surface is at the same height as the cantilever holder. During each sample height variation, the amplitudes of the undriven modes (first and third) are again magnitudes smaller than that of the driven mode (second).

Figure 24. Elastic-beam model driven at 2nd mode: tip displacement while scanning a flat sample surface (-22.7nm).

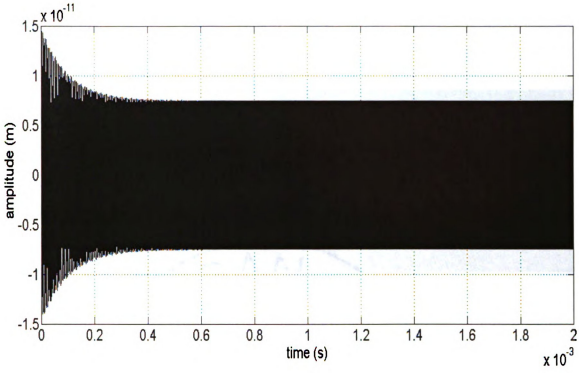

(a) first mode

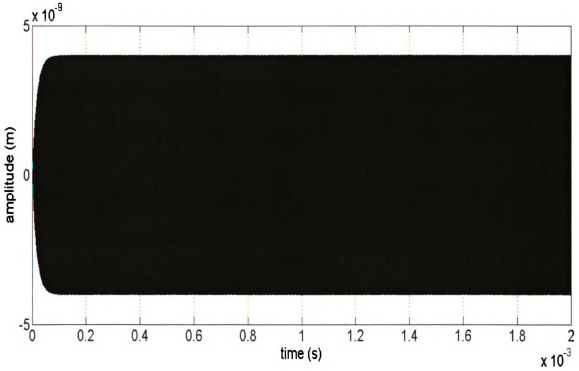

(b) second mode

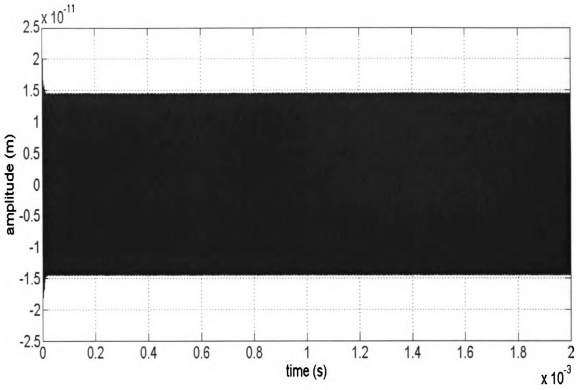

(c) third mode

Figure 24 continued.

Figure 25. Elastic-beam model driven at 2nd mode: tip displacement while scanning a varying sample surface height (-22.7nm to -4.5nm).

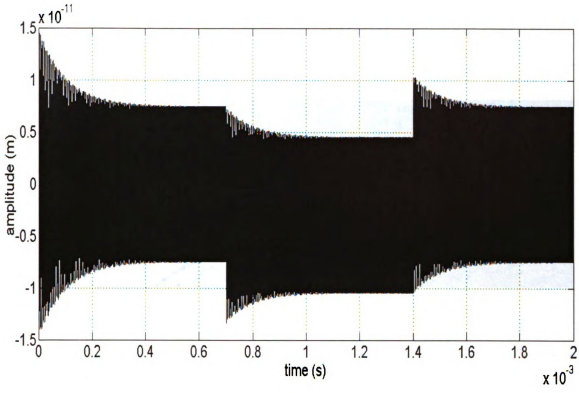

(a) first mode

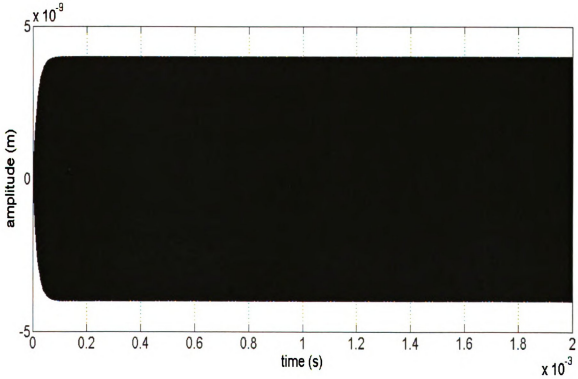

(b) second mode

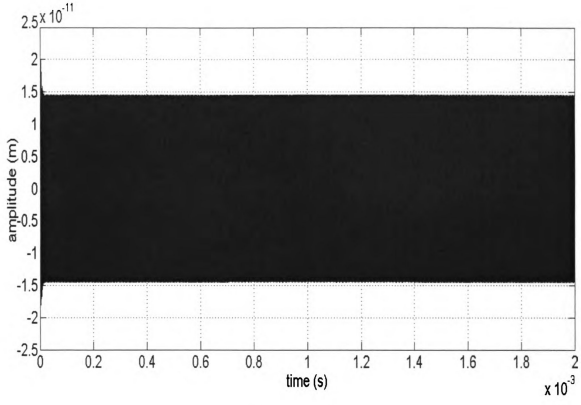

(c) third mode

Figure 25 continued.

Figure 26. Elastic-beam model driven at 2nd mode: tip displacement while scanning a varying sample surface height (-22.7nm to -4nm).

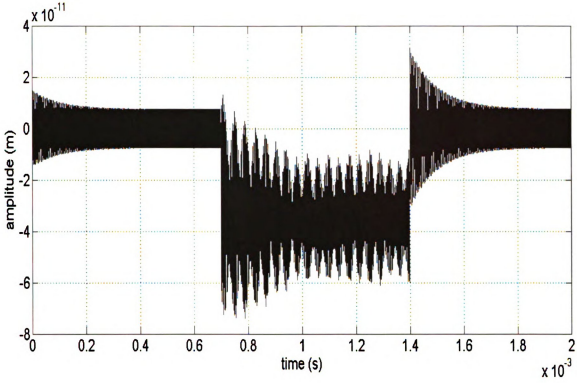

(a) first mode

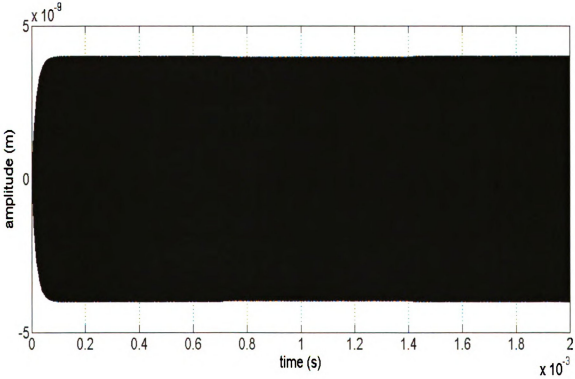

(b) second mode

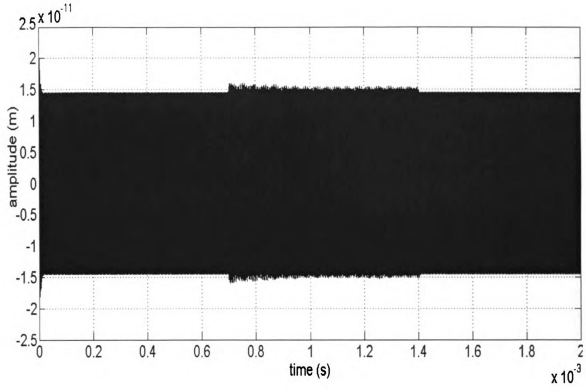

(c) third mode

Figure 26 continued.

Figure 27. Elastic-beam model driven at 2nd mode: tip displacement while scanning a varying sample surface height (-22.7nm to 0nm).

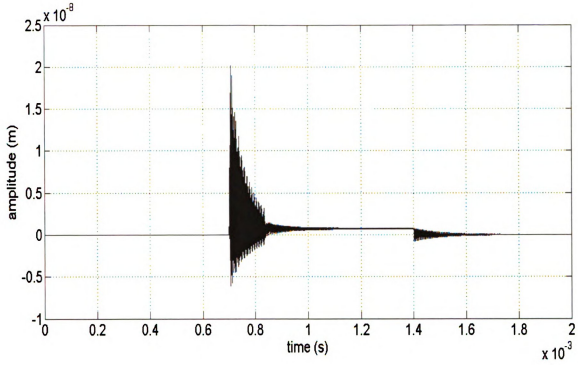

(a) first mode

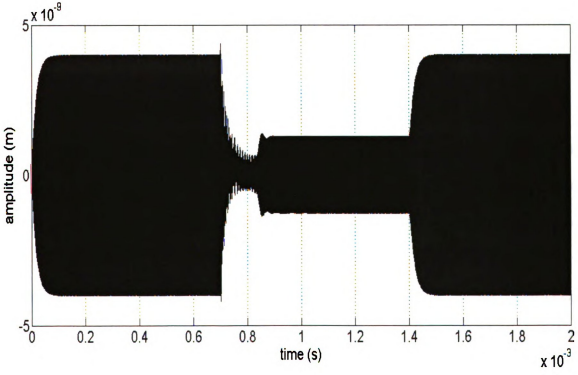

(b) second mode

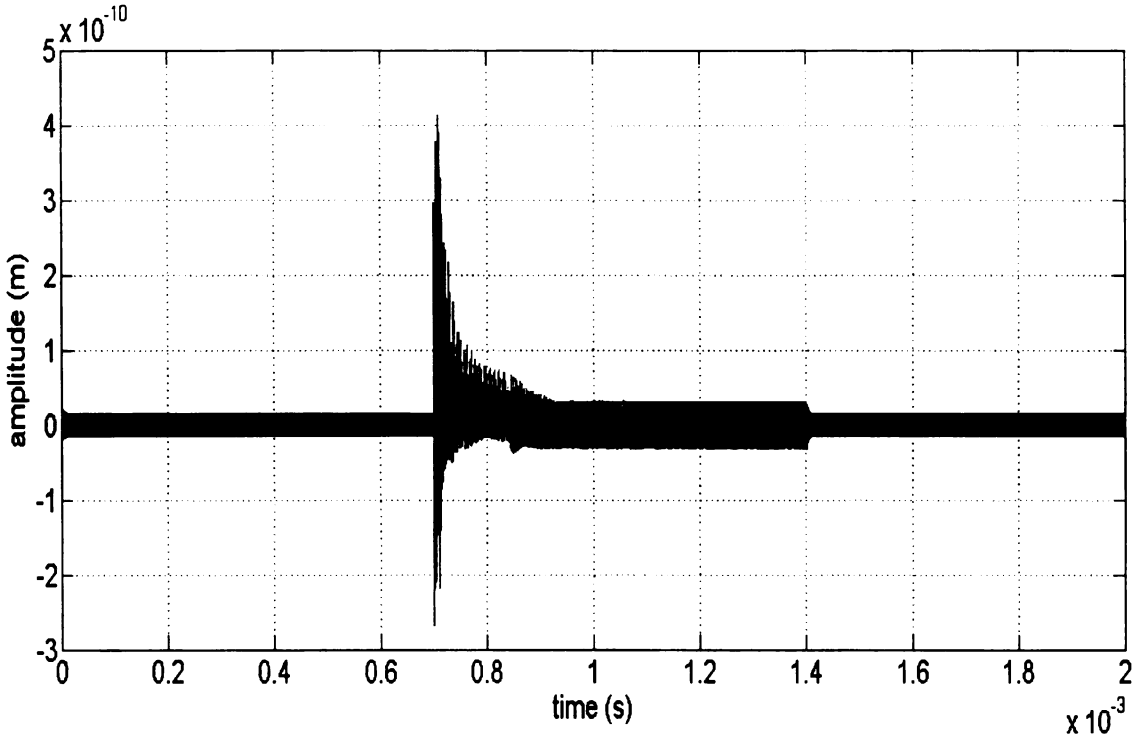

(c) third mode

Figure 27 continued.

4.2.3. Multiple Changes in Sample Topography

For the following simulation, the mode amplitude that was most sensitive to variations in specimen topography for each model was recorded. A 2-millisecond single-line scan simulation was performed on a computer-generated sample surface consisting of a bulge and depression in the topography. The specimen height was adjusted to -4nm midway through scanning, which was the point at which the tip tapped the surface in previous simulations. The sample was then heightened to -2nm to replicate a bulge and lowered to -6nm to replicate a depression in the surface (see Figure 28).

For the point-mass simulation, the cantilever was driven at the first resonance frequency while the first mode amplitude was recorded. The results in Figure 28 illustrate that the depression at -6nm is barely detectable. The amplitude change at the bulge is approximately -57% while that at the depression is approximately 29%.

Figure 28. Point-mass model: bulge and depression in sample surface.

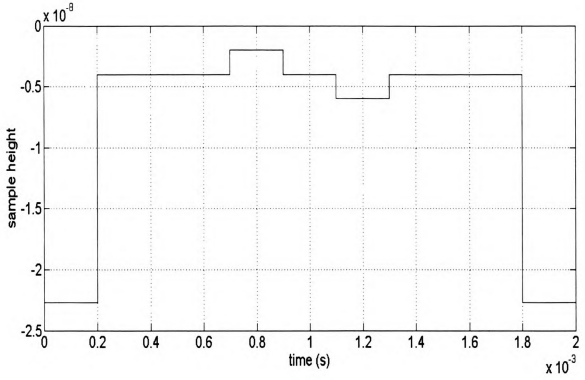

(a) sample

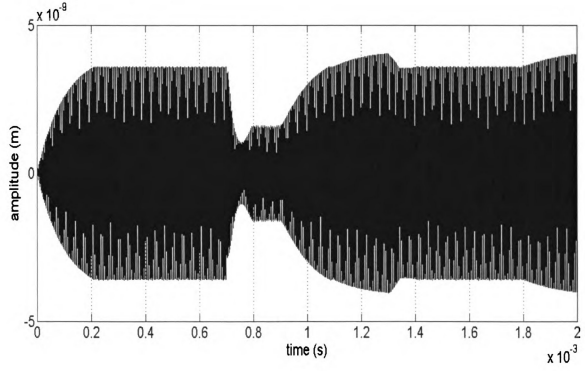

(b) first mode

The cantilever was then driven at the first resonance frequency while the second mode amplitude was recorded. As seen in Figure 29, the second mode is more sensitive to variations in sample topography. The amplitude during the bulge is more than 20 times the original amplitude; however, it quickly decays to a negligible size. Meanwhile, the amplitude during the depression is half the size of the original amplitude but is barely detectable.

Figure 29. Elastic-beam model driven at 1st mode: bulge and depression in sample surface and 2nd mode amplitude.

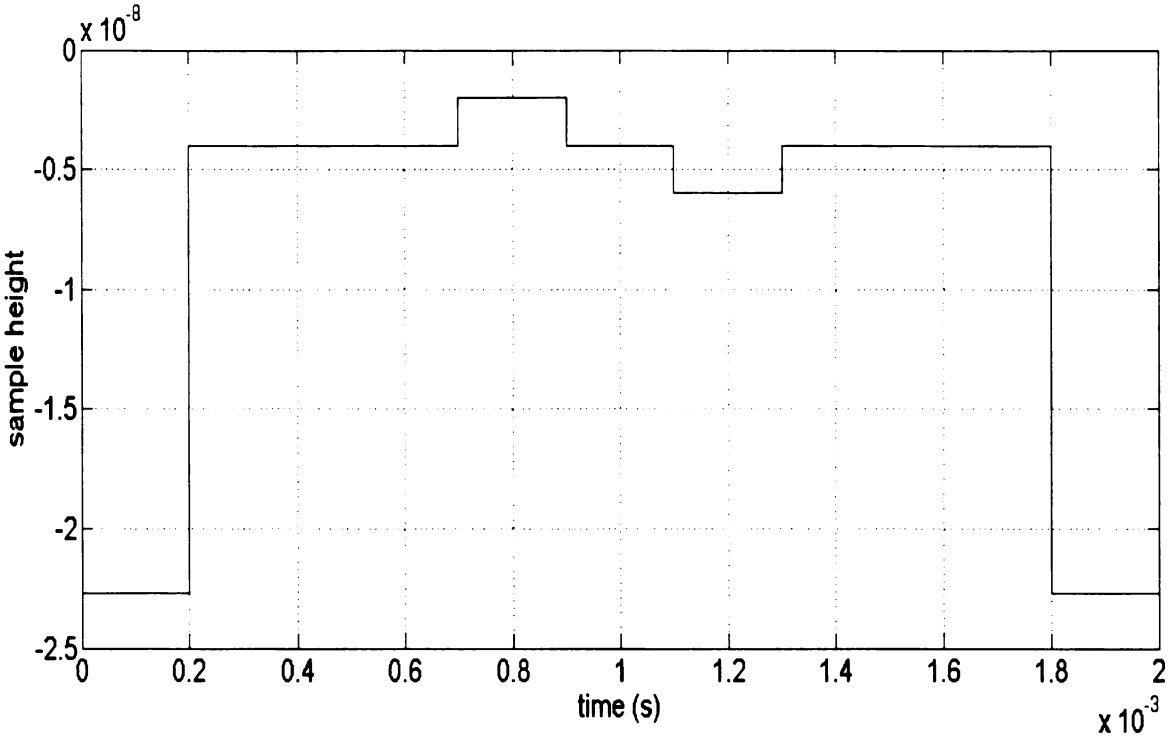

(a) sample

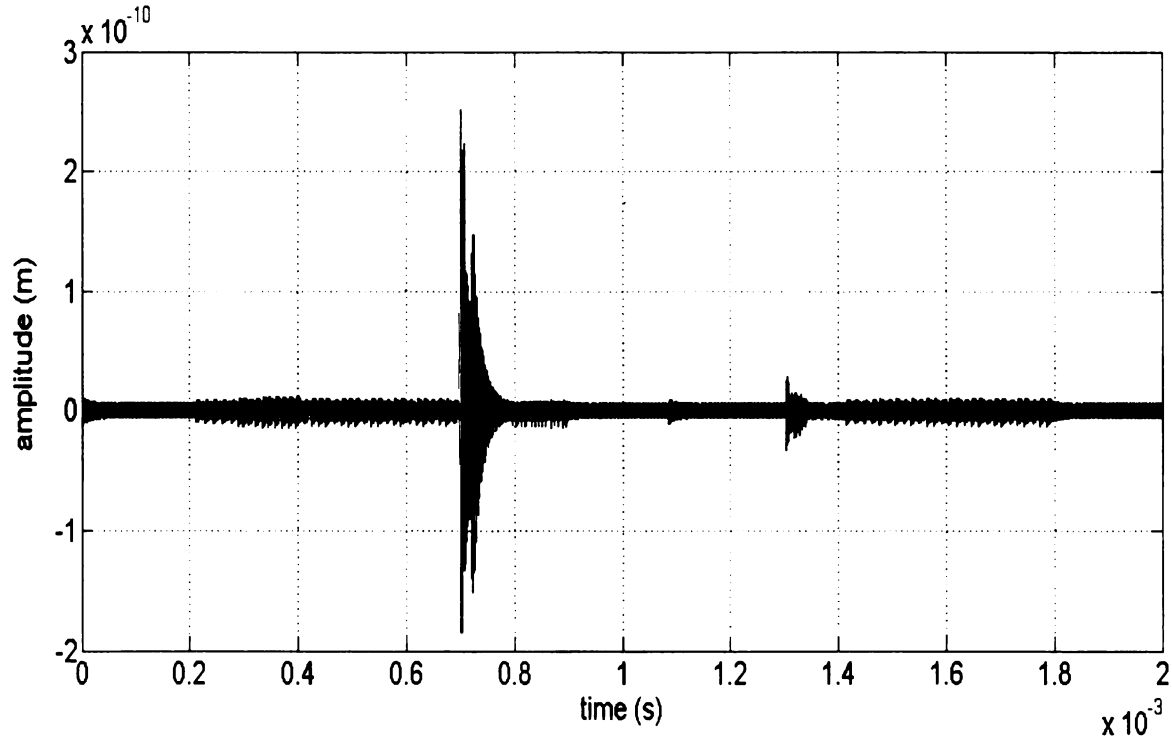

(b) second mode

A second elastic-beam simulation was performed in which the cantilever was driven at the second resonance frequency while the first mode amplitude was recorded. The results in Figure 30 show that the first mode is even more sensitive to multiple variations in sample topography. The amplitude change during the bulge is well more than 75 times the original amplitude initially; it then quickly decays to a steady 30 times. The amplitude change during the depression is barely noticeable since the cantilever is still recovering after having left the bulge.

Figure 30. Elastic-beam model driven at 2nd mode: bulge and depression in sample surface and 1st mode amplitude.

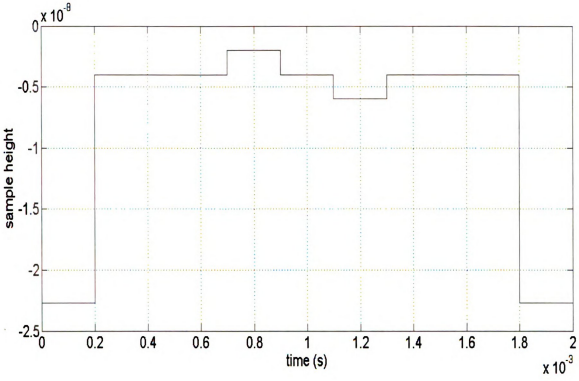

(a) sample

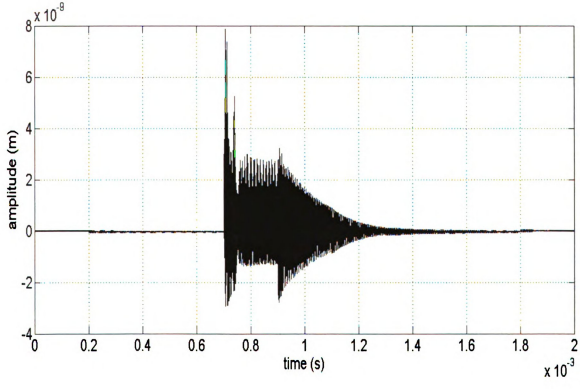

(b) first mode

4.3 DISCUSSION

4.3.1. Response to a Change in Sample Stiffness

The point-mass simulation, which considers the first mode alone, is unable to detect the changes in surface stiffness. For the elastic-beam simulation in which the cantilever is driven at the first resonance frequency, the first three modes are all also unable to detect such changes. Both simulation results are consistent with studies in which the 8^{th} harmonic, at a minimum, is necessary to sense surface stiffness variations.

The elastic-beam simulation in which the cantilever is driven at the second resonance frequency, on the other hand, detects the variations in surface stiffness. The first mode is significantly more sensitive to these variations than the third mode. This latter result may be due to the fact that the cantilever is more flexible, and thus easier for surface forces to excite, at lower harmonics. The second mode, however, is unable to detect any of the changes in surface stiffness. Since the cantilever is driven at the second resonance frequency, the amplitude of the second mode is dominated by the driving force amplitude.

4.3.2. Response to a Change in Sample Topography

When the cantilever is driven at the first resonance frequency, the second and third modes of the elastic-beam simulation are more able to detect changes in sample topography than the point-mass model. This result is consistent with theoretical and experimental studies demonstrating that certain sample surface information may be

omitted when examining the first mode alone. Additionally, the second mode of the elastic-beam simulation is more sensitive than the third. This observation is again consistent with the cantilever being more flexible and, thus, easier to excite at lower harmonics.

Meanwhile, for the elastic-beam simulation in which the cantilever is driven at the second resonance frequency, the second harmonic is least sensitive to sample topography variation. This result is due to the fact that the oscillation amplitude of the second mode is dominated by the driving force amplitude, as was the case in sample stiffness variation. The first and third modes are more able to identify the surface topography changes. The first mode, however, is more sensitive to these changes since the cantilever is more flexible at lower harmonics.

4.3.3. Multiple Changes in Sample Topography

The point-mass simulation is again least sensitive to the variations in sample topography. Though the elastic-beam simulation was more sensitive to these variations, when the cantilever was driven at the fundamental resonance frequency, the amplitude change of the higher (second) mode was difficult to distinguish over the depression in the specimen surface. When the cantilever was driven at the second resonance frequency, the first mode sensitivity was magnitudes greater than the second mode in the previous run. This result is consistent with the theory that lower modes are more responsive to changes in the sample surface since the cantilever is more flexible, and thus easier to excite, at these lower modes.

5. EXPERIMENT IMPLEMENTATION AND TESTING

5.1 DESCRIPTION OF EXPERIMENT IMPLEMENTATION

An atomic force microscope with a DMASP active probe (Veeco Instruments) was used to verify the sample topography results obtained in the computer simulations. The specimen in this experiment was an electrode on a silicon substrate and its height was approximately 30nm. The first mode amplitude of the cantilever was measured by a DSP lock-in amplifier (Stanford Research Systems, 102 kHz bandwidth). Nanoscope (Veeco), which is a program that records images of the sample height and second mode amplitude, was modified to also generate an image of the first mode amplitude. The cantilever (probe) holder was fixed at a height of approximately 4nm above the specimen surface.

5.2 EXPERIMENTAL RESULTS

The cantilever was driven at the first and second resonance frequencies. Images of the specimen height, first mode amplitude, and second mode amplitude were generated while the second mode was used as a feedback signal. (The AFM was designed by Veeco to use the second mode vibration as feedback.) The results show that when the cantilever is driven at the first resonance frequency, the first and second mode amplitudes are almost indistinguishable (see Figure 31). However, when the cantilever is driven at the second resonance frequency (see Figure 32), the specimen surface features are more visible in the first mode amplitude than the second mode. Moreover, a comparison of the first mode amplitudes in Figure 31b and in Figure 32b reveals that the first mode displays

more features via the dark spots when driving the cantilever at the second resonance frequency (see Figure 32b).

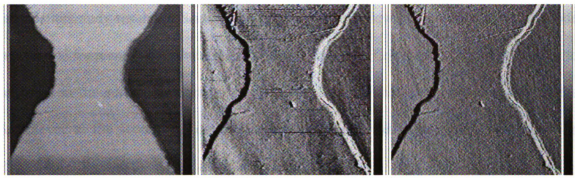

(a) (b) (c)

Figure 31. Image results while exciting the cantilever at the 1st mode. (a) height information, (b) first mode amplitude, (c) second mode amplitude.

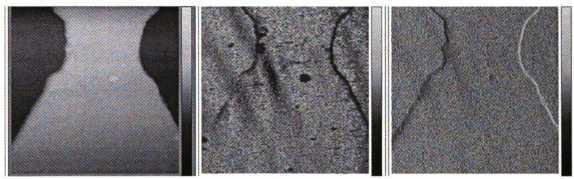

(a) (b) (c)

Figure 32. Image results while exciting the cantilever at the 2nd mode. (a) height information, (b) first mode amplitude, (c) second mode amplitude.

5.3 DISCUSSION

The first harmonic is more sensitive to specimen features when the cantilever is driven at the second frequency as opposed to the first. This result confirms the computer simulation study results in Section 4.2.2; when the cantilever is driven at a higher mode resonance frequency, the lower modes (in this case, the first mode) become sensitive to changes in the surface topography. However, it is difficult to tell whether driving the cantilever at the second resonance yields significantly better results as determined in Section 4.2.3 given the nature of the image results.

6. CONCLUSION AND FUTURE WORK

6.1 CONCLUSION

Simulation results demonstrate that examining higher modes yields more accurate information about a specimen surface – particularly elasticity and topography – which is consistent with previous studies. More importantly, this research achieves improved sensitivity to surface information in lower modes when exciting the cantilever at a higher resonance frequency.

The latter finding presents a potential alternative to extracting and enhancing the amplitudes of higher modes, which are magnitudes smaller and consequently more difficult to measure and analyze. By investigating lower modes instead, accurate specimen surface information can still be obtained while avoiding the implementation of amplitude enhancement. The findings of this research suggest improved imaging of specimen with varying surfaces, which is beneficial in the analysis of polymer films, DNA strands, semiconductor materials, and other samples in nanotechnology-related research.

6.2 FUTURE WORK

Future studies may investigate a wide range of topographically varying specimen while driving the cantilever at the first and second resonance frequencies. Image comparisons may then reveal more concrete experimental evidence as to the benefit of examining lower mode amplitudes while driving the cantilever at a higher mode frequency. Also,

development of a high bandwidth lock-in amplifier may be explored to better detect higher mode amplitudes for imaging.

Additionally, studies may investigate changes in the harmonic phase signals while exciting the cantilever at a higher resonance frequency. It is already common practice in atomic force microscopy to examine the phase (in addition to the amplitude) for sample surface information when driving the cantilever at the fundamental resonance frequency alone [3].

7. APPENDIX: COMPUTER SIMULATION CODE

The following two pieces of code were written to implement the elastic-beam model into the Veeco AFM tapping mode simulation package. The following code calls numerous other modules which are not included in this Appendix.

RunMe2Simulate.m – Code run before each simulation.

Declares and initializes cantilever and tip-specimen force parameters; Euler-Bernoulli Beam Equation variables; other important parameters.

```
clear;
clear global;

global idx;
global index;
global tspan;
tspan = zeros(1,40002);

global w_L2
global w_L2dot
global Tip_Pos_Min
global Tip_Pos_Max
global Amplitude


%%%%%%%%%%%%%%%%%%%%%%%%
global H   % the Hamaker constant, used in the DMT model
global R   % the tip radius, used in the DMT model
global a0  % interatomic distance, used in the DMT model
global Estar  % the effective contact stiffness, used in
the DMT model
global gamma  % in DMT model


global L  % Length of the cantilever
global m
global rho  % density of the cantilever
global A    % area of the cross section of the cantilever
global E    % Young's modules of the cantilever
global I    % Inertia of the cantilever

global omega % Eigenfrequency of the cantilver
global L1    % Position of the drive force acting point
global L2    % Position of the tip-sample interaction
acting point
```

```
global Number_of_Modes % Number of the modes
global TipPos  %Tip position

global zeta     % the damping coefficient of each mode
global KL       % Used to calculate the eigenfrequencies,
omega(i) = KL(i)^2/(L^2) * sqrt( E*I/(rho*A) );
global phi_L1    % modeshapes of the cantilever at L1
global phi_L2    % modeshapes of the cantilever at L2
global CurrentSamplePos % current Sample Position
global Drive_omega
global Drive_Force_Amp   % Amplitude of the driving force

global IntegralOfModeShapes
global d_on
global d_off
global gamma_1
global h_1
global IsMeniscusPresent

global ResidueMode

global Fcap
global Fts
global HolderPos

global IndxDrive
global Et
global nuet
global Es
global nues
global V_1
global r_1
global W

Pgain = 1;
Dgain = 1;

Number_of_Modes = 7; %5; %8;
IndxDrive = 1; %2;


% Some parameters are from Physical Review B 69, 085412
(2004) by Robert W Stark
% Use non-normalized mode shapes to avoid numerical
difficulty.
% Since normalized mode shapes would be very large and they
have unit
```

```
% of 1/sqrt(kg) , and modal coordinates would be very small
and they have
% unit of m*sqrt(kg).

R = 20e-009; %m % nm
Et = (1.3e11); %*(1e-15)*(1000); % mN/(nm)^2   % the
elastic moduli of tip, in DMT
nuet = 0.3; % no unit                % the poisson rations
of tip, in DMT

L = (125e-6); %/(1e-9); % nm
W= (35e-6); %/(1e-9); % nm
rho = (2.33e3); %*(1e-9)^3; % kg/(nm)^3   density of
silicon
A = (4e-6)*(35e-6); %/( (1e-9)^2 ); % (nm)^2 %4e-6 * 250e-
6;
m = rho*A; % kg/nm
E = (1.31e11); %*(1e-15)*(1000); % mN/(nm)^2
I = (1/12) * (35e-6) * ( (4e-6)^3 ); % / ((1e-9)^4); %
(nm)^4 %(1/12)*(250e-6)*(4e-6)^3;


%Sample parameters
Es = 7e10; %*(1e-15)*(1000); % mN/(nm)^2       % the
elastic moduli of sample, in DMT
nues = 0.3; % no unit                % the poisson rations
of sample, in DMT
gamma = (31e-3); %*(1e-6); % (pJ)/(nm)^2
H = (6.4e-20); %/(1e-12); % pJ
a0 = (1.65474e-10); %/(1e-9); % nm   % sqrt(
H/(24*pi*gamma) );


Estar = 1/( (1-nuet^2)/Et  + (1-nues^2)/Es ); %*(1000); %
mN/(nm)^2

%Capillary force parameters
h_l=2e-10; % / (1e-9); %[nm] %Water film thickness
gamma_l=0.072; %*(1e-6); %[pJ/nm^2] %liquid-vapor
interfaccial energy for water
r_l=(3*pi*gamma*R^2/Estar)^(1/3);
V_l=4*pi*R*h_l^2 + 4/3*pi*h_l^3 + 2*pi*r_l^2*h_l;
d_on=2*h_l;    %Tip-sample distance to form the water
meniscus
d_off=V_l^(1/3)-1/(5*R)*V_l^(2/3);    %Tip-sample distance
to break the water meniscus
```

```
IsMeniscusPresent = 0;

L1 = (1/10)*L; % nm
L2 = L;% (0.999999)*L; % nm


[omega,KL] =
GetEigenFrequencies(Number_of_Modes,L,E,I,rho,A);

IntegralOfModeShapes = testInteg(KL,L);


Drive_omega = omega(IndxDrive);

phi_L1 = getModeShape(L1,KL,L);
phi_L2 = getModeShape(L2,KL,L);


zeta(1:Number_of_Modes+1)=1/200;

%%%%%%%%%%%%%%%%%%%%%%%%%%%%

%totalSteps = 300000;
totalSteps = 40002; %100000;
%%%%%%%%%%%%
%Phase_of_Tip = zeros(1, totalSteps);
Amplitude = zeros(1, totalSteps);
Tip_Pos_Max = zeros(1, totalSteps);
Tip_Pos_Min = zeros(1, totalSteps);
w_L2 = zeros(1, totalSteps);
w_L2dot = zeros(1, totalSteps);
```

Sfcn_AFM.m – S-function ("cantilever" block in Section 4).

Simulates the cantilever as it oscillates in response to driving and tip-sample forces; and scans a simulated sample surface.

```
function [sys,x0,str,ts]= sfcn_AFM(t,x,u,flag)

switch flag

  %%%%%%%%%%%%%%%%%%
  % Initialization %
  %%%%%%%%%%%%%%%%%%
  case 0
    [sys,x0,str,ts] = mdlInitializeSizes();;

  %%%%%%%%%%
  % Update %
  %%%%%%%%%%
  case 2,
    sys = mdlUpdate(t,x,u);

  %%%%%%%%%%
  % Output %
  %%%%%%%%%%
  case 3
    sys = mdlOutputs(t,x,u);

  %%%%%%%%%%%%
  % Terminate %
  %%%%%%%%%%%%
  case 9
    sys = []; % do nothing

  otherwise
    error(['unhandled flag = ',num2str(flag)]);
end


%
%=============================================================
==================
% mdlInitializeSizes
% Return the sizes, initial conditions, and sample times
for the S-function.
%=============================================================
==================
%
```

```
function [sys,x0,str,ts]=mdlInitializeSizes();

% New globals
global w_L2;
global w_L2dot;

global w1_L2;
global w1_L2dot;


global Tip_Pos_Min;
global Tip_Pos_Max;
global HolderPos;

global Drive_omega

global Amplitude;
global tspan

global Number_of_Modes;
global idx;

idx = 1;

tspan(1) = 0;


q = 0*ones(1,Number_of_Modes);
qdot = 0*ones(1, Number_of_Modes);

w_L2(1) = 0; %Tip position
w_L2dot(1) = 0; %Tip velocity

w1_L2(1) = 0;
w1_L2dot(1) = 0;

Tip_Pos_Max(1) = 0;
Tip_Pos_Min(1) = 0;
HolderPos = 0; %22.7e-9; %0; %5e-9; %10e-9; %22.7e-9;

Amplitude(1) = 0; %2e-11;

fai = 0;
%%% Calculate the phase angle
fai =  atan2(Drive_omega*(w_L2(1)-
(Tip_Pos_Max(1)+Tip_Pos_Min(1))/2), w_L2dot(1))-
Drive_omega*tspan(1);
```

```
fai = fai- floor(fai/(2*pi))*2*pi;
if (fai>pi)
    fai = fai-2*pi;
end
fai = fai- pi/2.0;
Phase_of_Tip(1) = fai;

%%%

sizes = simsizes; %1
sizes.NumContStates  = 0;
sizes.NumDiscStates  = Number_of_Modes*2+5+3;
sizes.NumOutputs     = 8; %4; %4; %Number_of_Modes*2+2+1;
sizes.NumInputs      = 3;
sizes.DirFeedthrough = 0;
sizes.NumSampleTimes = 1;

sys = simsizes(sizes); %1x7

for k = 1:5
    w_L(k) = 0;
end

x0  = [transpose([q, qdot]); transpose(w_L); w_L2dot(1);
Phase_of_Tip(1); Amplitude(1)];
str = [];
ts  = [5e-8 0];

% end mdlInitializeSizes

%
%============================================================
==================
% mdlUpdate
% Handle discrete state updates, sample time hits, and
major time step
% requirements.
%============================================================
==================
%
function sys = mdlUpdate(t,x,u);

global TipPos  %Tip position
global phi_L2    % modeshapes of the cantilever at L2
global CurrentSamplePos % current Sample Position
global Drive_omega
global Drive_Force_Amp   % Amplitude of the driving force
```

```
global IntegralOfModeShapes
global HolderPos

% New globals
global w_L2
global w_L2dot

global w1_L2
global w1_L2dot

global Tip_Pos_Min
global Tip_Pos_Max
global Amplitude

global idx
global tspan

global Number_of_Modes

Drive_Force_Amp = u(1);
HolderPos = u(2);
CurrentSamplePos = u(3);


q = transpose(x(1:Number_of_Modes));  % 1x2
qdot = transpose(x(Number_of_Modes+1:Number_of_Modes*2));
% 1x2

idx = idx+1;
tspan(idx) = t;

[q, qdot] = rk4(2, tspan(idx-1),
tspan(idx),q,qdot,Number_of_Modes,0);  %sys =
transpose(RK4(1,idx-1,idx+1,q,qdot,Number_of_Modes,0));  %
DOESN'T WORK

%InteractionForce = Fts;
%CapillaryForce = Fcap;

TipPos = 0;
w_L2dot(idx) = 0;

for j = 1:Number_of_Modes
    TipPos = TipPos + phi_L2(j)*q(j);
    w_L2(idx) = TipPos;
    w_L2dot(idx) = w_L2dot(idx) + phi_L2(j)*qdot(j);
```

```
end

%%%%% Calculate the contour of the vibration
if w_L2dot(idx-1)<=0 && w_L2dot(idx)>0
    Tip_Pos_Min(idx-1) = w_L2(idx-1);
end

if w_L2dot(idx-1)>=0 && w_L2dot(idx)<0
   Tip_Pos_Max(idx-1) = w_L2(idx-1);
end
%
Tip_Pos_Min(idx) = Tip_Pos_Min(idx-1);
Tip_Pos_Max(idx) = Tip_Pos_Max(idx-1);

Amplitude(idx) = Tip_Pos_Max(idx) - Tip_Pos_Min(idx);
%1.15e-8;


%%% Calculate the phase angle
fai =  atan2(Drive_omega*(w_L2(idx)-
(Tip_Pos_Max(idx)+Tip_Pos_Min(idx))/2), w_L2dot(idx))-
Drive_omega*tspan(idx);
fai = fai- floor(fai/(2*pi))*2*pi;
if (fai>pi)
    fai = fai-2*pi;
end
fai = fai- pi/2.0;
Phase_of_Tip(idx) = fai;

%%%

for k = 1:2 %1:Number_of_Modes
    w_L(k) = phi_L2(k+5)*q(k+5);
end
for k = 3:5
    w_L(k) = 0;
end



sys = [transpose([q, qdot]); transpose(w_L); w_L2dot(idx);
Phase_of_Tip(idx); Amplitude(idx)];

%
%=============================================================
==================
% mdlOutputs
```

```
% Return the output vector for the S-function
%=============================================================
==================
%
function sys = mdlOutputs(t,x,u)

global Number_of_Modes;
global idx;
global HolderPos;

M1 = zeros(8, 2*Number_of_Modes);
M2 = eye(8,8); %[1 0 0 0; 0 1 0 0; 0 0 1 0; 0 0 0 1];
sys = [M1, M2]*x;

% end mdlOutputs
```

8. REFERENCES

[1] Sahin, O., Quate, C. F., Solgaard, O., and Atalar, A., "Resonant harmonic response in tapping-mode atomic force microscopy," *Physical Review B*, vol. 69, 2004.

[2] Zypman, F. R. and Eppell, S. J., "Analysis of scanning force microscope force-distance data beyond the Hookian approximation," *Journal of Vacuum Science & Technology B: Microelectronics and Nanometer Structures*, vol. 16, no. 4, pp.2099-2101, July 1998.

[3] Balantekin, M. and Atalar, A., "Enhancing higher harmonics of a tapping cantilever by excitation at a submultiple of its resonance frequency," *Physical Review B*, vol. 71, no. 12, 2005.

[4] Zhang, J., Xi, N., Li, G., and Su C., "Atomic Force Microscopy Sensing Using Multiple Modes,".

[5] Hillenbrand, R., Stark, M., and Guckenberger, R., "Higher harmonics imaging in tapping-mode atomic-force microscopy: Insights into the tip-sample interaction," *Applied Physics Letters*, vol. 76, no. 23, June 2000.

[6] Stark, R. W. and Heckl, W. A., "Higher harmonics imaging in tapping-mode atomic-force microscopy," *Review of Scientific Instruments*, vol. 74, no. 12, Dec. 2003.

[7] Rodriguez, T. R. and Garcia, R., "Compositional mapping of surfaces in atomic force microscopy by excitation of the second normal mode of the microcantilever," *Applied Physics Letters*, vol. 84, no. 3, Jan. 2004.

[8] Rabe, U., Janser, K., and Arnold, W., "Vibrations of free and surface-coupled atomic force microscope cantilevers: Theory and experiment," *Review of Scientific Instruments*, vol. 67, no. 9, pp. 3281-3293, Sept. 1996.

[9] Garcia, R. and San Paulo, A., "Attractive and repulsive tip-sample interaction regimes in tapping-mode atomic force microscopy," Physical Review B, vol. 60, no. 7, Feb. 1999.